Research

Investigation of Peroxisome Proliferator-Activated Receptor Genes as Requirements for Visual Startle Response Hyperactivity in Larval Zebrafish Exposed to Structurally Similar Per- and Polyfluoroalkyl Substances (PFAS)

Sebastian Gutsfeld,[1] Leah Wehmas,[2] Ifeoluwa Omoyeni,[1] Nicole Schweiger,[1] David Leuthold,[1] Paul Michaelis,[1] Xia Meng Howey,[2] Shaza Gaballah,[2] Nadia Herold,[1] Carolina Vogs,[3,4] Carmen Wood,[2] Luísa Bertotto,[2] Gi-Mick Wu,[5] Nils Klüver,[1] Wibke Busch,[1] Stefan Scholz,[1] Jana Schor,[6] and Tamara Tal[1,7]

[1]Department of Bioanalytical Ecotoxicology, Chemicals in the Environment Research Section, Helmholtz-Centre for Environmental Research–UFZ, Leipzig, Germany
[2]Center for Computational Toxicology and Exposure, Office of Research and Development, US Environmental Protection Agency, Research Triangle Park, North Carolina, USA
[3]Department of Biomedical Science and Veterinary Public Health, Swedish University of Agricultural Sciences, Uppsala, Sweden
[4]Institute of Environmental Medicine, Karolinska Institutet, Stockholm, Sweden
[5]Research and Development Institute for the Agri-Environment, Quebec, Quebec, Canada
[6]Department of Computational Biology and Chemistry, Chemicals in the Environment Research Section, Helmholtz-Centre for Environmental Research–UFZ, Leipzig, Germany
[7]Medical Faculty, University Leipzig, Leipzig, Germany

BACKGROUND: Per- and polyfluoroalkyl Substances (PFAS) are synthetic chemicals widely detected in humans and the environment. Exposure to perfluorooctanesulfonic acid (PFOS) or perfluorohexanesulfonic acid (PFHxS) was previously shown to cause dark-phase hyperactivity in larval zebrafish.

OBJECTIVES: The objective of this study was to elucidate the mechanism by which PFOS or PFHxS exposure caused hyperactivity in larval zebrafish.

METHODS: Swimming behavior was assessed in 5-d postfertilization (dpf) larvae following developmental (1–4 dpf) or acute (5 dpf) exposure to 0.43–7.86 μM PFOS, 7.87–120 μM PFHxS, or 0.4% dimethyl sulfoxide (DMSO). After developmental exposure and chemical washout at 4 dpf, behavior was also assessed at 5–8 dpf. RNA sequencing was used to identify differences in global gene expression to perform transcriptomic benchmark concentration–response (BMC$_T$) modeling, and predict upstream regulators in PFOS- or PFHxS-exposed larvae. CRISPR/Cas9-based gene editing was used to knockdown peroxisome proliferator-activated receptors (ppars) *pparaa/ab*, *pparda/db*, or *pparg* at day 0. Knockdown crispants were exposed to 7.86 μM PFOS or 0.4% DMSO from 1–4 dpf and behavior was assessed at 5 dpf. Coexposure with the ppard antagonist GSK3787 and PFOS was also performed.

RESULTS: Transient dark-phase hyperactivity occurred following developmental or acute exposure to PFOS or PFHxS, relative to the DMSO control. In contrast, visual startle response (VSR) hyperactivity only occurred following developmental exposure and was irreversible up to 8 dpf. Similar global transcriptomic profiles, BMC$_T$ estimates, and enriched functions were observed in PFOS- and PFHxS-exposed larvae, and ppars were identified as putative upstream regulators. Knockdown of *pparda/db*, but not *pparaa/ab* or *pparg*, blunted PFOS-dependent VSR hyperactivity to control levels. This finding was confirmed via antagonism of *ppard* in PFOS-exposed larvae.

DISCUSSION: This work identifies a novel adverse outcome pathway for VSR hyperactivity in larval zebrafish. We demonstrate that developmental, but not acute, exposure to PFOS triggered persistent VSR hyperactivity that required *ppard* function. https://doi.org/10.1289/EHP13667

Introduction

Per- and polyfluoroalkyl substances (PFAS) are a diverse class of synthetic chemicals containing >14,000 unique structures used in industrial manufacturing (US EPA PFASSTRUCTv3, last checked December 2023[1]). PFAS have surfactant-like, water-resistant, and flame-retardant properties[2,3] and are widely used in packaging products, nonstick cookware coatings, and firefighting foams.[4] Given their chemical stability, PFAS are mostly resistant to degradation processes,[5] which leads to their wide detection in the environment (e.g., Gawor et al.,[6] Rankikn et al.,[7] Pan et al.[8]), wildlife,[9,10] and humans.[11–13] Toxicity effects associated with exposure to perfluorooctanesulfonic acid

(PFOS) or perfluorohexanesulfonic acid (PFHxS) include endocrine disruption, immunotoxicity, developmental toxicity, developmental neurotoxicity (DNT), and cardiovascular toxicity in rodent and human cell models.[14,15] PFOS was added to Annex B of the Stockholm Convention on Persistent Organic Pollutants in 2009. PFHxS was added to Annex A of the Stockholm Convention without exemptions in 2023 (EU Regulation 2019/1021, Decision SC10/13). In 2023, the US Environmental Protection Agency (EPA) proposed a National Primary Drinking Water regulation for six PFAS, including PFOS and PFHxS.[16] PFOS and PFHxS accumulate in the brains of humans, wildlife, and in exposed laboratory animals (reviewed by Cao and Ng[17]) and PFAS exposure during early stages of development is associated with altered behavior in humans.[18–21] Studies using early life–stage zebrafish have shown that exposure to PFAS caused a diversity of behavioral effects[22–26] and had structure-dependent trends in chemical bioconcentration.[27–29] We and others have identified alkyl sulfonic acids as a particularly bioaccumulative subclass of PFAS that triggered dark-phase locomotor hyperactivity in larval zebrafish light–dark transition tests.[27–29] A systematic comparison of aliphatic sulfonic acid PFAS data revealed that potency for dark-phase hyperactivity increased with longer carbon chain length.[23,29] Based on these findings, we hypothesized that exposure to structurally similar alkyl sulfonic acid PFAS, such as PFOS and PFHxS, cause hyperactivity via a shared molecular mechanism.

One strategy to investigate the chemical mode of action is the use of genetically modified zebrafish lines that experience either target gene knockout or an overrepresentation of gene function. Individual

Note to readers with disabilities: *EHP* strives to ensure that all journal content is accessible to all readers. However, some figures and Supplemental Material published in *EHP* articles may not conform to 508 standards due to the complexity of the information being presented. If you need assistance accessing journal content, please contact ehpsubmissions@niehs.nih.gov. Our staff will work with you to assess and meet your accessibility needs within 3 working days.

fish lines can be generated by injecting a single Cas9/guide RNA (gRNA) complex into a single-cell–stage zebrafish embryo.[30] A key constraint of this strategy is that two to three generations of adult animals are required to obtain homozygous mutants.[30] A recent alternative approach to the creation of stable knockout lines is to generate F0 knockdown zebrafish embryos.[31] This strategy used multiple guide RNAs per gene to generate F0 functional knockdown zebrafish larvae in a single day[31] and was therefore considered convenient for rapid hypothesis testing in larval zebrafish.

In the present study, we used the Clustered Regularly Interspaced Short Palindromic Repeats (CRISPR)/Cas9-based gene knockdown to identify putative causal links between exposure to PFOS or PFHxS, genes encoding peroxisome proliferator-activated receptors (*ppars*), and multiple hyperactivity phenotypes. This study dissected behavior phenotypes that arise from developmental or acute exposure and paired RNA sequencing (RNA-seq), gene editing, and pharmacological manipulation to ultimately reveal a novel mechanism by which these widely occurring environmental chemicals trigger visual startle response (VSR) hyperactivity in larval zebrafish.

Methods

UFZ Zebrafish Husbandry

Except for the RNA-seq study, performed at the US EPA, all data was generated at the UFZ, where all procedures involving zebrafish (*Danio rerio*) were approved by Landesdirektion Leipzig Aktenzeichen (75-9185.64; TVV41/19; TVV 61/20) and carried out in accordance with relevant guidelines and regulations. Strain TL adults were housed in 26-L glass tanks at an approximate density of 3 fish/L. Physicochemical parameters of the aquaria water were frequently measured (pH 7–8; water hardness 2–3 mmol/L, nitrate <2.5 mg/L, nitrite <0.025 mg/L, ammonia <0.6 mg/L, oxygen saturation 87%–91%). Adults were fed dry food (Special Diets Services) twice daily and shell-free artemia (Sanders) once daily Mondays through Fridays. Both food sources were fed once on weekends. Zebrafish were maintained on a 14:10 light:dark cycle at 28.5°C and bred every 1–2 wk by placing breeding trays in on-rack glass tanks. The following morning, embryos were collected. Fertilized and normally developed embryos were selected[32] with a dissection microscope (Olympus SZx7-ILLT). For gene editing experiments, sex-segregated breeds were transferred to 2.6-L divided tanks with one female and two males. The following morning, inserts containing the fish were placed in fresh rack water, and dividers were sequentially pulled between 0800 and 1200 hours. Inserts were routinely changed to fresh bottom tanks to collect single-cell–stage embryos for microinjections.

Chemical Preparation

PFOS [Chemical Abstracts Service Registry No. (CASRN): 1763-23-1; CAT# 6164-3-08] and PFHxS (CASRN: 3871-99-6; CAT# 6164-3-X4) were purchased from Synquest Laboratories (purities >99.9%). Stock solutions (20 mM) were prepared by dissolving neat powder into anhydrous dimethyl sulfoxide (DMSO; Sigma-Aldrich). Aliquots were stored at −80°C until use. In line with previous work,[29] for each experiment, 250-fold working solutions were prepared by thawing single-use stock solution aliquots and performing quarter-log serial dilutions in DMSO in a 96-well polycarbonate microtiter plate prepared <12 h before use and discarded after each experiment. For repeat exposure experiments performed at the US EPA for RNA-seq analysis, and in line with previously published work,[29] stock plates containing 250-fold working solutions were sealed (Biorad MSB1001) and stored at room temperature in the dark, used for the duration of each experiment, and then discarded.

Study Design and Chemical Exposure (UFZ)

To stay in line with our previous work,[29] we opted to bleach embryos to reduce microbial burden and reduce associated decrements in embryo and larval development. At day 0, zebrafish embryos were bleached using a 0.05% sodium hypochlorite (NaOCl) solution. Until plating, bleached embryos were kept at a density of 1 embryo per 2 mL of 10% Hanks' Balanced Salt Solution (10% HBSS) in glass crystallization dishes at 28°C. For all experiments (excluding the ppard antagonist-PFOS coexposure study), at 1 d postfertilization (dpf), single embryos were placed into each individual well of a 96-square well clear polystyrene plate (Whatman microplate devices, Uniplate, CAT# WHAT7701-1651) with 400 μL of 10% HBSS. For all experiments, embryos were exposed by transferring 1.6 μL of 250-fold working solution to each well. This resulted in a final concentration of 0.4% DMSO for all groups, including the vehicle control. Cross-contamination between wells and evaporation was minimized using Microsealers (Biorad MSA5001) and by wrapping the plate with parafilm. Plates were incubated at 28°C on a 14:10 h light:dark cycle. Unless otherwise indicated, the chemical solution was removed at 4 dpf, before 1200 hours, replaced with 400 μL of 10% HBSS, and behavior was measured at 5 dpf, after which the larvae were visually assessed for general malformations (e.g., edemas, body axis defects), death, and swim bladder inflation. Malformed, dead, or larvae with uninflated swim bladders were not included in behavior assessments. We conducted four different exposure designs, described below. Replicate numbers are indicated in figure legends.

Developmental or acute exposure. To disentangle behavioral phenotypes, acute and developmental exposure experiments were conducted. For developmental exposures, zebrafish embryos were exposed to 0.43–7.86 μM PFOS or 7.87–120 μM PFHxS from 1–4 dpf. At 4 dpf, the exposure solution was removed by 1200 hours and replaced with 400 μL of 10% HBSS. For acute exposures, 5 dpf larvae were exposed to 0.43–7.86 μM PFOS for 60 min or to 44.8–160 μM PFHxS for 412 min before the behavior test. The time-of-peak-effect (i.e., exposure window) for PFHxS was determined using a series of consecutive behavior tests (Figure S1, *n* = 44 and 46). For acute exposures, the chemical was not removed prior to testing. Replicate numbers ranged from 15 to 43 (Figure 1) for developmental exposures and from 21 to 47 for acute exposures (Figure 2).

Crispant exposure. Zebrafish embryos that experienced CRISPR/Cas9-dependent gene knockdown (i.e., crispants; details in the section "CRISPR/Cas9 Gene Editing Strategy") were developmentally exposed (1–4 dpf) to 7.86 μM PFOS or 0.4% DMSO in 96-square well plates (Whatman microplate devices, Uniplate, CAT# WHAT7701-1651). The level 7.86 μM of PFOS was selected because it provoked VSR hyperactivity in earlier concentration–response experiments (Figure 1C). At 4 dpf, the exposure solution was removed before 1200 hours and replaced with 400 μL of 10% HBSS. Replicate numbers ranged from 10 to 74 (Figure 7).

Depuration exposure (i.e., chemical washout). Embryos were exposed to 2.48–7.86 μM PFOS, 44.8–120 μM PFHxS, or 0.4% DMSO from 1 to 4 dpf in 96-square well plates (Whatman microplate devices, Uniplate, CAT# WHAT7701-1651). At 4 dpf, before 1200 hours, larvae were transferred in 20 μL of exposure solution to 48-round well plates (TPP Techno Plastic Products, Switzerland) containing 1 mL of 10% HBSS without PFAS chemicals. To remove the residual chemical, 800 μL of media was removed and replaced with 1 mL of 10% HBSS for a total volume per well of 1.2 mL. Microtiter plates were placed in the incubator at 28°C. Daily, between 5 and 8 dpf, 700 μL were removed from each well, and following a 2-h acclimation period, behavior was measured. Postbehavior, 700 μL of 10% HBSS containing Gemma Micro 75 food (Skretting Zebrafish) was

added to each well. Replicate numbers ranged from 23 to 48 ([Figure 3](#)).

Prolonged exposure to PFOS. To determine the effect of prolonged PFOS exposure, at 1 dpf, zebrafish were statically exposed to 0.38–12.0 μM PFOS or 0.4% DMSO in T25 tissue cultured flasks containing 15 embryos in 25 mL of exposure media. From 5 to 8 dpf, 80% media exchanges containing PFOS or DMSO and feeding (as previously described) were performed daily. At 8 dpf, media that did not contain PFOS or DMSO was used and the animals were fed. At 9 dpf, the larvae were transferred to 48-well plates in chemical-free media and stored in the dark for at least 2 h at 28°C prior to behavior testing (Figure S2).

ppard antagonist coexposure. To mimic CRISPR/Cas9 study conditions where knockdown occurred at 0 dpf and chemical exposure commenced at 1 dpf, embryos were bleached, plated, and exposed to the ppard antagonist GSK3787 (3.14–80 μM) or 0.4% DMSO at 0 dpf. At 1 dpf, the embryos were exposed to 7.86 μM PFOS or 0.4% DMSO, and the exposure solution was removed and replaced with 400 μL of 10% HBSS at 4 dpf. Replicate numbers ranged from 16 to 55 ([Figure 8](#)).

Automated Behavior Assay

On the day of testing, microtiter plates containing zebrafish larvae were transferred in the dark to an incubator set to 28°C, with lights off in the behavior testing room. After a minimum of 45 min, plates were transferred to the behavior machine (ZebraBox, ViewPoint) and a protocol comprising a 20-min dark acclimation at 0 lux, followed by testing in 20-min light at 13,238 lux [light phases 1, 2 (L1, L2)] and 22-min dark at 0 lux [dark phases 1, 2 (D1, D2)] was run. Zebrafish locomotion was captured using an infrared camera and the tracking algorithm of the ZebraLab software (Viewpoint). Videos were recorded at 25 frames/s and movement data were obtained at 1-s intervals. Data visualization and analysis procedures are described below. The entire pipeline is available as a user-friendly set of functions (version 0.1; Zenodo; https://doi.org/10.5281/zenodo.11396730).

For photoperiod (phase) data analysis, the individual distance moved per larvae was summarized in 2-min intervals. Assay phases comprised 10-min periods as follows: light phase 1 (L1), light phase 2 (L2), dark phase 1 (D1), dark phase 2 (D2). Accordingly, for each assay phase (L1, L2, D1, D2), five × two-min-sums per larva were calculated. A model of distance moved was fitted, using a beta distribution because distances are bound by zero and a maximum. This value was calculated as 1.001 times the maximum distance moved by a single larva within each experiment. The nonlinear effect of time was modeled using smoothing splines. Concentration and phase were modeled as categorical variables, and their second-order interactions were included. Finally, because all larvae were repeatedly measured, variability between individuals was modeled as random effects. This was done using generalized additive mixed effects models (GAMMs[33]), implemented in the R package mgcv.

The model formula was as follows:

$$logit(distance\ moved) \sim s(time) + concentration + phase$$
$$+ concentration{:}phase + (1|animal) + \epsilon,$$

where
- $logit(distance\ moved)$ is the distance moved scaled from 0 to 1, and logit transformed
- $(time)$ is the smoothing spline for the trend through time, corrected for autocorrelation
- *concentration* is the categorical variable, the different concentrations tested
- *phase* is the categorical variable, the different assay phases

- *concentration*:*phase* is the second-order interaction of concentration and assay phase
- (1|*animal*) is the random effect, to control for variability between larvae and repeated measures design
- ε is the error term following a Beta distribution.

Model quality was assessed by visually inspecting residuals and fitted smooths for each model (Figures S3 and S4). Estimated marginal means (EMMs) based on the fitted model were calculated as post hoc tests. Obtained *p*-values were Tukey-adjusted to account for multiple comparisons. EMMs were calculated using the R package emmeans.[34] The VSR was calculated as the summed distance moved over the first 3 s after the dark–light (VSR1) or light–dark (VSR2) transitions. The VSR was modeled using a linear mixed effects model using lme4 package in R (R Development Core Team, v4.0.4).

The model formula was as follows:

$$startle\ response \sim concentration + startle\ phase + (1|animal) + \epsilon,$$

where:
- *startle response* is the startle response measured
- *concentration* is the categorial variable, the different concentrations tested
- *startle phase* is the categorial variable, either VSR1 or VSR2
- (1|*animal*) is the random effect, to control for variability between larvae and repeated measures design
- ε is the error term following a Gaussian distribution.

EMMs based on the fitted model were calculated as post hoc tests. Obtained *p*-values were Tukey-adjusted to account for multiple comparisons. EMMs were calculated using the R package emmeans. All statistical analyses and visualizations were done using custom-built scripts in R (version 4.0.4; R Development Core Team) and the following packages:
- Reshape2 (version 1.4.4[35])
- Ggplot2 (version 3.3.6[36])
- Car (version 3.0-11[37])
- Dplyr (version 1.0.7[38])
- Data.table (version 1.14.2[39])
- Openxlsx (version 4.2.5[40])
- multCompView (version 0.1-8[41])
- lme4 (version 1.1-27.1[42])
- emmeans (version 1.7.0[34])
- tidyverse (version 1.3.2[43])
- mgcv (version 1.8-33[33]).

CRISPR/Cas9 Gene Editing Strategy

F0 gene knockdown larvae (i.e., crispants) were generated for *pparg*, *pparaa/ab*, or *pparda/db*. The following sections describe the strategy and methods used for guide RNA selection, formation of guide RNA-adapter RNA duplexes, RNA duplex/Cas9 assembly into ribonuclear protein (RNP) triplexes, RNP pooling, and single-cell–stage microinjections (adapted from Kroll et al.[31]). In addition to the multiplexing strategy, and to increase data reproducibility, we opted to additionally include a second crispant group that included three different potential mutations in the same target genes. Therefore, six guide RNAs were designed to target each ppar gene at different loci. Two sets, each targeting three different loci on the gene, were microinjected in the two groups of embryos. Both sets were designed to disrupt gene function. Therefore, all behavior data generated with either set of crispants should be the same. As a control for the microinjection process, negative control (NC) crispants were microinjected with RNP complexes that contained guide RNAs that had no targets in the zebrafish genome.

Guide RNA selection. Guide RNAs were purchased from Integrated DNA Technologies (IDT; Alt-R CRISPR-Cas9 crRNA). Target site–specific guide RNAs were selected from the IDT database of predesigned guide RNAs for most annotated zebrafish genes (https://eu.idtdna.com/site/order/designtool/index/CRISPR_PREDESIGN). All guide RNA sequences are listed in Tables S1 and S2. For each target gene, guide RNAs were ranked based on predicted on-target and off-target scores. To increase the likelihood of inducing functional knockdown mutations, guide RNAs targeting anterior positions in early exons of the gene were selected. For the NC group, three guide RNAs that lacked targets in the zebrafish genome were selected (Alt-R CRISPR-Cas9 Negative Control crRNA #1, #2, #3; IDT). After each experiment, guide RNA efficiency was assessed as described below. New guide RNAs were designed as needed to ensure gene knockdown in subsequent studies (Table S2). Guide RNAs were individually resuspended in Duplex buffer (IDT) to form 200 μM stocks that were aliquoted and stored at −80°C until use.

Guide RNA duplex formation. Adapter RNA, termed tracrRNA, was also purchased from IDT (Alt-R CRISPR-Cas9 tracrRNA) and functioned to anneal to the guide RNA and bind the Cas9 protein. TracrRNA was resuspended in Duplex buffer (IDT) (200 μM), aliquoted, and stored at −80°C until use. For each experiment, guide RNA and tracrRNA were annealed to form 57 μM guide RNA duplex. Complexes were prepared by combining 1 μL of guide RNA 200 μM, 1 μL of tracrRNA 200 μM, and 1.51 μL of Duplex buffer. The mixture was heated to 95°C for 5 min followed by cooling on ice to induce annealing and formation of the guide RNA duplex.

Guide RNA/Cas9 RNP assembly. Cas9 Alt-R S.p. HiFi Cas9 Nuclease V3 was purchased from IDT (10 μg/mL or 61 μM). Cas9 working buffer was prepared using 20 mM Tris-HCl (Tris-hydrochloride), 600 mM potassium chloride, and 20% glycerol in ultrapure water. The pH was adjusted to 7.5 using sodium hydroxide (NaOH) then sterile-filtered (0.2-μm pores). Cas9 working buffer was aliquoted and stored at −20°C until use. Before each experiment, Cas9 protein was diluted in Cas9 working buffer to 57 μM. RNP complexes were prepared individually for each target site by combining 1 μL of diluted Cas9 protein with 1 μL of guide RNA duplex.

RNP pooling. One day prior to each experiment, three RNP pools were prepared for microinjections. For each crispant set (set 1–8 or NC), 2 μL of each assigned RNP were mixed, yielding a total volume of 6 μL (for *pparg*, NC) or 12 μL (for *pparaa/ab* or *pparda/db*). Pooled RNP complexes were stored overnight at 4°C until microinjections.

Single-Cell–Stage Microinjections

Prior to microinjections, RNP pools were mixed with 1 μL of filter-sterilized phenol red (Sigma-Aldrich) to facilitate injection success. Approximately 1 nanoliter of each RNP pool was injected into the yolk of embryos at the single-cell–stage, which comprised ∼28.5 fmol of guide RNA, 28.5 fmol of Cas9, and 28.5 fmol of total guide RNA. RNPs were present in equal amounts in the pool. Accordingly, in the case of three RNPs per set, 9.5 fmol of each RNP were coinjected.

NaOH-Based Lysis/DNA Extraction

DNA extraction of whole zebrafish larvae samples was performed using NaOH-based lysis.[44] Morphologically normal larvae were selected for DNA extraction. Prior to extractions, five anesthetized and euthanized larvae were pooled in 1.5-mL microcentrifuge tubes. Five to seven replicates were generated per crispant set (i.e., set 1–8 or NC). Excess medium was removed and the larvae were submerged in 100 μL of 50 mM NaOH (CASRN: 1310-73-2; Roth). Subsequently, pooled larvae in NaOH were heated to 95°C for 15 min. After heating, the tubes were cooled on ice to 4°C. After cooling, 10 μL of 1M Tris-HCl (pH 8.0) was added, followed by centrifugation at 5,000 rpm for 5 min at room temperature, then 100 μL of supernatant was transferred to a thermocycler plate, sealed with adhesive polymerase chain reaction (PCR) sealer, and stored at −20°C.

Primer Design

To evaluate the success of target gene disruption, primers were designed.[45] Briefly, individual primer pairs were designed for each target site (Tables S1 and S2). The left primer spanned the guide RNA target site. If mutations were induced at the target site, binding of the left primer was blocked, resulting in lower levels of the amplification product. Primers were designed using the online tool Primer 3[46] and purchased from Eurofins Genomics. After arrival, primers were diluted to 10 μM stocks with MilliQ water, according to the manufacturer's specifications, aliquoted, and stored at −20°C until use.

Quantitative Real-Time PCR

Gene knockdown efficiency was assessed using quantitative real-time PCR (qRT-PCR; Applied Biosystems StepOnePlus). Prior to amplification, the DNA content of lysed samples was measured using Qubit (ThermoFisher). To ensure equal starting amounts of DNA per reaction, DNA content was normalized to 1 ng/μL. Separate master mixes were created, one for each primer pair. Master mixes contained 3.25 μL of diethyl pyrocarbonate (DEPC)–treated water, 6.35 μL of Sensi Mix Hi-ROX (Bioline), 0.5 μL of left primer stock (Eurofins), 0.5 μL of right primer stock (Eurofins), and 2 ng of DNA in 2 μL. Three technical replicates for each sample were generated. One primer set per reaction was used. Samples were heated to 95°C, and held for 10 min followed by 40 cycles of 15 s at 95°C, 20 s at 53.5°C, 20 s at 72°C, 15 s at 95°C, and 1 min at 60°C, after which the samples were heated to 95°C in 0.3°C per 15-s steps. The ratio of Ct-values between the NC control and set 1–8 crispants were used to assess gene knockdown efficiency for each target site and analyzed using Wilcoxon signed rank tests.

Verification of **pparda/db** *Target Gene Knockdown Using DNA Sequencing*

DNA sequencing of gRNA target sites was used as an additional verification of gene knockdown efficiency. Refined sets comprising 5 gRNAs targeting *pparda/db* (Table S3; sets 9–10) were used for single-cell–stage microinjections, as described above. This comprised five cut sites located on exons *pparda* exon 2, *pparda* exon 3, *ppardb* exon 5, *ppardb* exon 6, and *ppardb* exon 8. At day 0, after microinjections, the zebrafish embryos were bleached using a 0.05% NaOCl solution. Bleached embryos were kept at a density of 1 embryo per 2 mL of 10% HBSS in glass crystallization dishes at 28°C until 5 dpf. At 5 dpf, the larvae were anesthetized by placing the glass dishes on ice for at least 20 min. Then, single larvae were collected in individual tubes and stored on ice after the removal of excess liquid. DNA extraction of single larvae samples was conducted using a DNeasy Blood and Tissue Kit (Qiagen), according to manufacturer instructions. DNA from 9 NC control individuals (Alt-R CRISPR-Cas9 Negative Control crRNA #1, #2, #3; IDT), 10 set 9, and 10 set 10 crispants targeting the *pparda/db* genes were amplified. DNA normalization and qRT-PCR were performed as described above in the section "Quantitative Real-Time PCR" using primers that flanked the cut sites (Table S3). PCR products with at least 4 ng/μL DNA were transferred to a PlateSeq Kit for crude PCR products (Eurofins Genomics) and shipped for sequencing using Sanger Sequencing (Eurofins

Genomics). Sequences derived from NC control individuals, where a majority of base calls had quality values >30, were included in the aligned results. Because gene editing in F0 crispants results in mosaicism, all crispant sequences were aligned to the controls. Sequence alignments were performed via the R package msa (version 1.30.1)[47] using ClustalW[48] and aligned against sequences for ENSDARG00000044525 (*pparda*) and ENSDARG00000009473 (*ppardb*) obtained from the GRCz11 Ensemble genome assembly (https://www.ensembl.org/Danio_rerio/Info/Index). Alignments were visualized using the seqvisr package in R (R Development Core Team, v4.0.4).[49]

US EPA Zebrafish Husbandry

All procedures involving zebrafish were approved by the US EPA National Health and Environmental Effects Research Laboratory Institutional Animal Care and Use Committee and carried out per the relevant guidelines and regulations. Embryos were obtained from a mixed wild-type adult zebrafish line (*D. rerio*) that was generated and maintained as previously described.[29] Zebrafish adults were housed in 6-L tanks at an approximate density of 8 fish/L. Adults were fed Gemma Micro 300 (Skretting) once daily and shell-free E-Z Egg (Brine Shrimp Direct) twice daily Mondays through Fridays. Both food sources were fed once daily on weekends. US EPA wild-type zebrafish were maintained on a 14:10 light:dark cycle at 28.5°C and bred every 2–3 wk. For embryo collection, 60–100 adults were placed in 10- or 20-L angled static breeding tanks overnight. The following morning, adults were transferred to new angled bottom tanks containing fish facility water, and embryos were collected 30–40 min later.

RNA-Seq Study Design and Chemical Exposure (US EPA)

At 0 dpf, zebrafish embryos were bleached as previously described.[50] Embryos at the dome to epiboly stages[32] were placed in individual wells of a 96-well plate containing a 40 μM nylon mesh filter (Millipore, CAT# MANMN4010) with 400 μL of 10% HBSS per well. Filter inserts containing zebrafish embryos were transferred to 96-well culture trays (Millipore, CAT# MAMCS9610) containing 250 μL of 10% HBSS and 1 μL of 250-fold working solutions per well (0.88–2.8 μL PFOS or 7.87–25.1 μM PFHxS). A final concentration of 0.4% DMSO was used for all exposure groups, including the vehicle control. Daily, from 1 to 5 dpf, plates underwent 100% media changes to refresh chemical dosing solutions by blotting (Brandel CAT#: FPXLR-196) and transferring mesh inserts containing zebrafish to new bottom 96-well plates (Millipore, CAT# MAMCS9610). To minimize evaporation, plates were sealed (Biorad CAT#: MSA5001) and wrapped with parafilm. Plates were maintained on a 14:10 light:dark cycle at 26.0°C. At 4 and 5 dpf, morphologically normal larvae were collected for head dissections followed by RNA-seq.

RNA Extraction from Zebrafish Head Tissue

Prior to dissections, zebrafish larvae were anesthetized for 10 min in ice-cold 10% HBSS. Scalpels were used to collect head tissue at 4 or 5 dpf, cutting anterior to the swim bladder. This included the lower jaw. Fifteen head tissue samples were pooled in 400 μL of 10% HBSS in 1.5-mL RINO Red Bead lysis microcentrifuge tubes (Next Advance). Eight biological replicates per treatment group were generated. After adding 450 μL of Trizol to each tube, the samples were homogenized at speed 8 for 3 min using a Bullet Blender Tissue Homogenizer (Next Advance). The samples were spun down at room temperature for 8 min at 12,000 g and stored on ice until subsequent RNA isolation. RNA was isolated from aqueous supernatant using a Direct-zol kit (Zymo Research, CAT# R2052) according to the manufacturer's protocol.

Isolated RNA was purified and enriched using RNA Clean & Concentrator Kit (Zymo Research, CAT# 1019) according to the manufacturer's protocol. Illumina Next Seq500 RNA-seq was performed by the Genomics Research Core at the National Health and Environmental Effects Research Laboratory (NHEERL).

RNA-Seq

RNA sample quality was checked by Bioanalyzer (Agilent Technologies, CAT# 2100) and concentrations were assessed by Qubit RNA BR kit (ThermoFisher, CAT# Q10211). Six samples per group, with RNA integrity number (RIN) values >9.0, were selected for use. Selected RNA samples were randomized and processed on Apollo324 for polyA selection (IntegenX), and then complementary DNA (cDNA) libraries were prepared with PrepX mRNA 48 Protocol (version 19; Takara Bio USA). PCR amplification with 16 index primers was run for 13 cycles. The resulting PCR products were cleaned up on Apollo324 with PCR Cleanup 48 Protocol (Takara Bio USA). The resulting PCR product quality was checked on Bioanalyzer with High Sensitivity DNA chips and the average size (in base pairs) was obtained according to an electropherogram. All samples had identifiable peaks between 250 and 290 bp. Collected libraries were quantified by Qubit DNA HS kit (ThermoFisher, CAT# Q32851). The molar concentration of each library was estimated by using average molecular size from Bioanalyzer data and concentration from Qubit measurement. An equal amount from each library (volume × concentration) was pooled from 16 randomized libraries to make the sequencing library pools (total 3 pools of 16 libraries each) and concentrations of the pooled libraries were checked by Qubit. All samples had a concentration >1 nM after pooling. Library pools were denatured and diluted according to Illumina NextSeq protocols. The final concentrations for sequencing were 2.5 pM +2% Phix and they were run for 75 cycles Single Read (SR). Q30 scores were at least 92.4% and there were >10 million total reads. The resulting sequencing data was stored on the Gene Expression Omnibus (GEO) repository under the identifiers GSE190490 (for PFOS) and GSE190009 (for PFHxS).

Gene Expression Analysis

Identification of differentially expressed genes. Illumina basecall files were converted to FASTQ format, demultiplexed by bcl2fastq2, and uploaded to Partek Flow (version 8.0.19.0428). Within Partek Flow, adapters were trimmed, and reads were quality filtered. Bases with Phred quality scores <20 were trimmed from either end and reads with lengths <25 nucleotides were removed. Trimmed and filtered FASTQ files were aligned to *D. rerio* GRCz11 using STAR (version 2.5.3a) with default settings in Partek Flow. Alignment resulted in an average of 31 million mapped reads ± standard deviation (SD) of 5.1 [coefficient of variation (CV) = 16%] with average base quality scores of 34 ± 2.0 (CV = 0.52%) and >91% alignment to the genome, of which $64 \pm 4.8\%$ were, on average, uniquely mapped. Gene counts were quantified from aligned reads by Partek Expectation Maximization using Ensembl *D. rerio* GRCz11.93, with a high percentage of reads mapping to exonic regions of the genome (>72%). Low expression genes across all samples were filtered if the geometric mean was ≤ 1. Sample gene counts were then normalized to library size using quantile normalization and $\log_2$ transformed prior to differential gene expression analysis with Partek Gene Specific Analysis (GSA). GSA uses a multi-model approach and the lowest corrected Akaike information criterion (AIC) to identify the best response distribution (lognormal, normal, negative binomial, or lognormal with shrinkage) for the data. Contrasts for PFHxS and PFOS included all concentrations vs. control. Genes were considered differentially expressed genes (DEGs) if they had a $p < 0.05$ and an absolute binary logarithmic base 2 fold change ($\log_2 FC$) value >1.5.

Prediction of upstream regulators. For pathway analysis and upstream regulator prediction, significant *D. rerio* genes were converted to human orthologs using biomaRt (version 2.34.2) in R (version 3.4.3; R Development Core Team). Please note that human PPARs are denoted throughout using capital letters while, in line with common nomenclature standards, zebrafish ppar genes are denoted using lowercase letters. For multiple identified orthologs (i.e., one *Homo sapiens* gene to many *D. rerio*), those considered "high confidence" (i.e., percentage identity of ≥ 50, gene order conservation score of ≥ 75, and whole genome alignment score of ≥ 75) were given precedence in a 1:1 ratio. If a high confidence ortholog was not identified, then the ortholog with the highest percentage identity between the *D. rerio* and *H. sapiens* was selected in a 1:1 ratio. Gene order conservation scores were calculated by determining how many of the four nearest neighboring genes match between orthologous pairs and whole genome alignment scores to calculate the coverage of alignment in regions surrounding the orthologs pairs (https://useast.ensembl.org/info/genome/compara/Ortholog_qc_manual.html/#hc, last accessed 6 February 2020). Significantly enriched canonical pathways and upstream regulators were identified from the *H. sapiens* orthologs in Ingenuity Pathway Analysis (IPA; version 01-06, Qiagen). Significant enrichment was identified by Fisher's exact test ($p < 0.05$) or an absolute value z-score ≥ 2.

Benchmark concentration analysis. Benchmark concentration (BMC) analysis was used to estimate the threshold concentration at which specific genes were differentially expressed. Transcriptional BMC analysis of head RNA-seq data was conducted using BMDExpress (version 2.2).[51] The low expression filtered, normalized, and $\log_2$-transformed count matrixes for each chemical and time point were loaded into BMDExpress using Ensembl zebrafish identifiers. Filtering and analyses followed general recommendations provided by the National Toxicology Program (NTP) Research Report on National Toxicology Program Approach to Genomic Dose-Response Modeling[52] with minor changes. Briefly, genes were analyzed by analysis of variance (max absolute $\log_2$FC >1.5, $p < 0.05$) to identify treatment-related effects. To identify concentration–responsive genes, significant genes were then fit to the following models: Hill, power, linear, 2° and 3° polynomial models, exponential 2, exponential 3, exponential 4, and exponential 5 models. Each model was run assuming constant variance with a 0.95 confidence level. The benchmark response factor was set to 1.349 times the standard deviation in the control animals and power restricted to ≥ 1.[53] For best-fit polynomial model selection, a nested likelihood ratio test was performed on the linear and polynomial models. If the more complex model provided a significantly improved fit ($p < 0.05$), the more complex model was selected. The simpler model was selected if the more complex model did not provide a significantly improved fit.[54] Models with a global goodness-of-fit $p < 0.1$ were excluded. To select the best globally fitting model with the least complexity, the AIC for the selected polynomial model was then compared with the AIC for the Hill and power models. The model with the lowest AIC was selected as the final model. The Hill model was flagged if the k parameter was $<1/3$ the lowest positive concentration and then the next best model with a fit of $p > 0.05$ was used. If no other best-fit model could be identified when the Hill model was flagged, the Hill model was retained. Genes with a transcriptomic BMC value greater than the highest exposure concentration were excluded.[55] Modeled genes were then compared with Gene Ontology Biological Process (GOBP) to identify significantly enriched gene sets using the BMDExpress functional classification. To be included, gene sets needed to have a minimum of three overlapping genes with the GOBP and a Fisher's exact test two-tailed, $p < 0.05$. Genes also needed to have a ratio of the upper bound BMC (95th percentile; BMCU) to lower bound BMC (95th percentile; BMCL) <40. The median of the lowest enriched GOBP was used to set the overall transcriptomic BMC as a conservative indicator of biological activity for comparison with the behavior response.

Global analysis of gene expression using the zebrafish self-organizing map. To visualize and compare responses on a transcriptome-wide scale, we used the zebrafish embryo (ZFE) toxicogenomic universe map.[56] The self-organizing map (SOM) was based on a large training dataset of zebrafish embryo toxicogenomic data and is a two-dimensional grid of 60×60 nodes, each containing up to 54 genes. Genes were arranged on the map based on their expression profiles in the training data where genes within the same node or arranged in nodes in close proximity were coexpressed in different exposure scenarios. Map nodes were clustered and a functional enrichment analysis on these clusters confirmed enrichments for certain biological functions in specific regions of the map. New data can be projected onto the map to identify up- or down-regulated parts of the transcriptome and to compare the effects of different chemicals. Linear modeling was used to identify DEGs using a treatment vs. control contrast (R package limma version 3.52.5[57]). To increase statistical power, individual concentrations were combined for each test chemical and at each time point. Unadjusted p-values with a threshold of 0.1 were used to define DEGs. Binary logarithmic fold changes (i.e., logFCs) of DEGs with $p > 0.1$ were set to zero so that only those with $p < 0.1$ influenced the SOM. SOMs were then generated by calculating mean logFCs for all nodes according to the assignment of genes to nodes in the toxicogenomic universe and visualized using R package ggplot2.[36]

Global analysis of gene expression using INfORM. The INfORM analysis tool was used to identify responsive modules of gene expression patterns[58] in PFOS- or PFHxS-exposed larvae, relative to the control. Prior to the analysis, gene names were converted to Human Genome Organisation (HUGO) Gene Nomenclature Committee (HGNC) symbols.[59] DEGs were calculated with a treatment vs. control contrast ($p < 0.05$ and log2FC ± 1.5). The normalized expression matrix of all DEGs served as input for the INfORM network analysis to identify walktraps of coexpressed genes.[58] The resulting walktrap data was used to conduct an analysis of overrepresentation using the Kyoto Encyclopedia of Genes and Genomes (KEGG)[60] and the Gene Ontology databases.[61,62] In addition, gene set enrichment analyses for the Gene Ontology and Reactome pathway data of each walktrap were performed using the INfORM analysis tool.[58]

Toxicity prioritization index determination. Half-maximal effect concentration (AC_{50}) data for 9,542 chemicals were retrieved from the current public release of the US EPA ToxCast project (invitrodb; version 3.5[63]). Relevant PFAS chemicals were obtained using a US EPA research list of PFAS (EPAPFASINV) retrieved from the CompTox Chemicals Dashboard (https://comptox.epa.gov/dashboard/). Potency profiles of PFAS chemicals tested in PPAR-relevant assays were calculated based on AC_{50} values and visualized using a toxicity prioritization index (ToxPi) analysis where all assays were weighed equally.[64] ToxPi scores for PFOS and PFHxS were extracted and visualized using ggplot2 package in R (version 3.3.6; R Development Core Team).

Results

Identification of DNT Phenotypes

We tested for DNT phenotypes using a light–dark transition test. Each of the four assay phases was 10-min long and the zebrafish larvae were subjected to light (L1, L2), or no light (D1, D2). In this
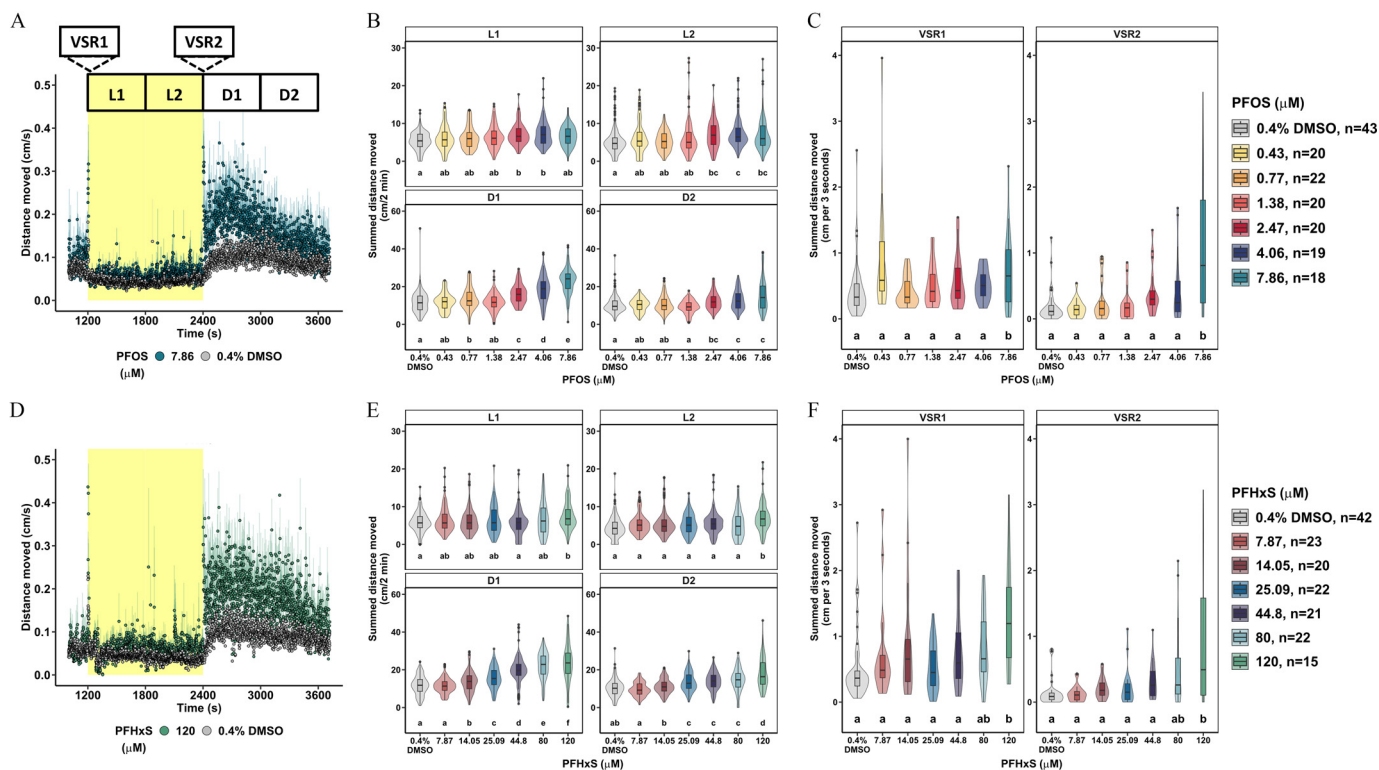
Figure 1. Locomotor activity assessment in 5-dpf zebrafish developmentally exposed to PFOS or PFHxS. Locomotor response following exposure to (A) 7.86 μM PFOS (blue), (D) 120 μM PFHxS (green), or 0.4% DMSO (gray) in the light (yellow)–dark (white) transition test. Data expressed as the mean distance moved (cm/s) ± standard error and represent 15–43 larvae per group. (B,E) Distance moved (cm) for each larva in 2-min periods across each 10-min light phase at 13,238 lux (L1, L2) and dark phase at 0 lux (D1, D2). Data are represented as box and violin plots. Violins around the box plots describe the kernel probability density of the underlying data. Significance was determined by Tukey-adjusted estimated marginal means following a generalized additive mixed effects model. Significant differences ($p < 0.05$) between groups are indicated by different letters. VSR data [within 3 s after dark–light (VSR1) or light–dark transition (VSR2)] following developmental exposure to (C) 0.43–7.86 μM PFOS, or (F) 7.87–120 μM PFHxS are also shown. Data are represented as box and violin plots and comprise 1 value per larva for VSR1 and VSR2. Significance was determined by Tukey-adjusted estimated marginal means following a linear mixed effects model. Significant differences ($p < 0.05$) between groups are indicated by different letters. Individual box plots comprise a box that describes the IQR, a bold line that represents the median, and whiskers that indicate the calculated minimum (25th percentile −1.5× IQR) and the calculated maximum (75th percentile +1.5× IQR). Dots represent outliers beyond the calculated minima or maxima. Violins around the box plots describe the kernel probability density of the underlying data. Replicate numbers tested for PFOS ranged from 18 to 43 larvae (C) and from 15 to 42 larvae for PFHxS (F). Summary data can be found in Excel Tables S1–S4. Note: D, dark; DMSO, dimethyl sulfoxide; dpf, days postfertilization; IQR, interquartile range; L, light; PFHxS, perfluorohexanesulfonic acid; PFOS, perfluorooctanesulfonic acid; VSR, visual startle response.

study, we introduced an additional end point, the VSR, defined as the distance moved over the first 3 s after the dark–light (VSR1) or light–dark (VSR2) transition (Figure 1A). Relative to the DMSO control, zebrafish larvae exposed to PFOS exhibited hyperactivity in the L1 (2.47–4.06 μM), L2 (2.47–7.86 μM), D1 (0.77 μM, 2.47–7.86 μM), and D2 (2.47–7.86 μM) periods (Figure 1B). In addition, VSR hyperactivity was observed in larvae exposed to 7.86 μM PFOS (Figure 1C). Similar to PFOS, hyperactivity was observed in larvae developmentally exposed to PFHxS in the L1 (120 μM), L2 (120 μM), D1 (14.05–120 μM), and D2 (14.05–120 μM) periods (Figure 1E), as well as in the VSR1 and VSR2 end points (120 μM) (Figure 1F), as compared with the DMSO control (Figure 1F).

Acute Neurotoxicity Phenotypes in PFOS- or PFHxS-Exposed Larval Zebrafish

To determine whether the D1 and VSR2 hyperactivity phenotypes were linked, we tested whether exposure to PFOS or PFHxS can acutely affect these stereotypic behaviors. PFOS-exposed larvae exhibited hyperactivity 60 min postexposure in the D1 (2.48–7.86 μM) and D2 (4.4, 7.86 μM) phases (Figure 2B). For PFHxS, we evaluated the relationship between exposure time and behavioral effects (Figure S1). Similar to PFOS, larvae

acutely exposed to PFHxS exhibited hyperactivity 412 min post-exposure in the L1 (146.4 μM), L2 (44.8–146.4 μM), and D1 (146.4 μM) periods (Figure 2E). Acute exposure to 0.43–7.86 μM PFOS or 44.8–160 μM PFHxS had no effect on the VSR end points (Figure 2C,F).

Systematic Characterization of DNT Phenotypes

Because we observed dark-phase (i.e., D1) hyperactivity following both developmental (Figure 1B,E) and acute (Figure 2B,E) exposure to PFOS or PFHxS, but only observed VSR2 hyperactivity following developmental exposure to the compounds (Figure 1C, F), we hypothesized that the D1 hyperactivity phenotype occurs via an acute, receptor-mediated mechanism, whereas the VSR2 phenotype has a developmental origin. To test this hypothesis, we performed a depuration (i.e., chemical washout) study, where larvae were developmentally exposed to 2.48–7.86 μM PFOS, 44.8–120 μM PFHxS, or 0.4% DMSO from 1 to 4 dpf. After chemical removal at 4 dpf, locomotor activity was assessed at 5, 6, 7, and 8 dpf (Figure 3A). Differences in hyperactivity responses were observed in the D1 and VSR2 periods (Figure 3B–E). Larvae developmentally exposed to PFOS exhibited concentration-dependent hyperactivity in the D1-phase at 5 dpf (2.48–7.86 μM) and 6 dpf (2.48–7.86 μM) (Figure 3B). By 7 dpf, the
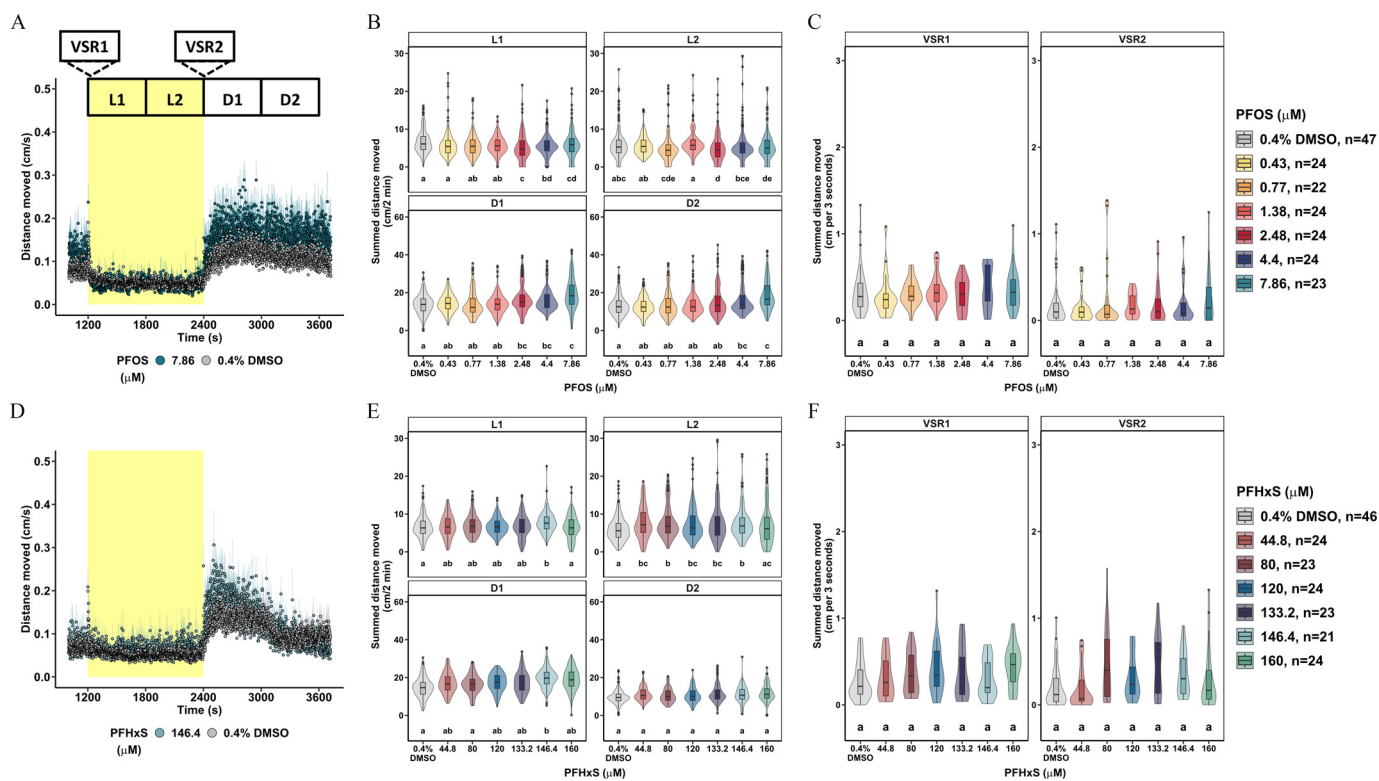
Figure 2. Locomotor activity assessment in 5-dpf zebrafish acutely exposed to PFOS or PFHxS. Locomotor response following acute exposure to (A) 7.86 μM PFOS (blue), (D) 146.4 μM PFHxS (green), or 0.4% DMSO (gray) in the light–dark transition test. Data expressed as the mean distance moved (cm/s) + standard error and represent 21–47 larvae per group. (B,E) Distance moved (cm) for each larva in 2-min periods across each 10-min light phase at 13,238 lux (L1, L2) and dark phase at 0 lux (D1, D2). Data are represented as box and violin plots comprising five values per larva in L1, L2, D1, D2. Violins around the box plots describe the kernel probability density of the underlying data. Significance was determined by Tukey-adjusted estimated marginal means following a generalized additive mixed effects model. Significant differences ($p < 0.05$) between groups are indicated by different letters. VSR data [within 3 s after dark–light (VSR1) or light–dark transition (VSR2)] following acute exposure to (C) 0.43–7.86 μM PFOS, or (F) 44.8–160 μM PFHxS are also shown. Data are represented as box and violin plots that comprise 1 value per larva for VSR1 and VSR2. Significance was determined by Tukey-adjusted estimated marginal means following a linear mixed effects model. Significant differences ($p < 0.05$) between groups are indicated by different letters. Individual box plots comprise a box that describes the IQR, a bold line that represents the median, and whiskers that indicate the calculated minimum (25th percentile $-1.5 \times$ IQR) and the calculated maximum (75th percentile $+1.5 \times$ IQR). Dots represent outliers beyond the calculated minima or maxima. Violins around the box plots describe the kernel probability density of the underlying data. Replicate numbers tested for PFOS ranged from 23 to 47 larvae (C) and from 21 to 46 larvae for PFHxS (F). Summary data can be found in Excel Tables S5–S8. Note: D, dark; DMSO, dimethyl sulfoxide; dpf, days postfertilization; IQR, interquartile range; L, light; PFHxS, perfluorohexanesulfonic acid; PFOS, perfluorooctanesulfonic acid; VSR, visual startle response.

concentration–response relationship was lost, and at 8 dpf, larvae exposed to 7.86 μM PFOS were no longer hyperactive relative to the DMSO control (Figure 3B). In contrast to the observed transient D1 hyperactivity, persistent and irreversible VSR2 hyperactivity was observed in larvae exposed to 2.48–7.86 μM PFOS from 5 to 8 dpf (Figure 3C). Similar to PFOS, at 5 dpf, larvae developmentally exposed to 44.8–120 μM PFHxS displayed concentration-dependent D1 hyperactivity, as compared with the DMSO control (Figure 3D), and again in line with the PFOS data (Figure 3B), by 7 and 8 dpf, concentration-dependent D1-hyperactivity was no longer present and, in some cases, activity levels returned to baseline (Figure 3D). In contrast to the D1 end point and analogous to PFOS-exposed larvae, we observed persistent concentration–response hyperactivity in the VSR2 from 5 to 8 dpf for larvae exposed to 44.8–120 μM PFHxS (Figure 3E). These data suggest two distinct phenotypes: *a*) that exposure to PFOS or PFHxS caused transient and reversible D1 hyperactivity, and *b*) that exposure to PFOS or PFHxS caused persistent and irreversible VSR2 hyperactivity. In support of this, prolonged exposure (1–8 dpf) to PFOS resulted in VSR hyperactivity but not D1 hyperactivity (Figure S2). Because this study was aimed at uncovering mechanisms by which these chemicals cause DNT-related effects, the VSR2 phenotype is the focus of the remainder of the report.

Transcriptomic Identification of Putative PFAS Mode of Action

To test the hypothesis that PFOS- or PFHxS-dependent VSR2 hyperactivity arose based on a developmental perturbation during neurodevelopment, a hypothesis generation study was conducted to identify putative upstream regulators that might causally regulate the hyperactivity effects in exposed larvae. Three strategies, including a global analysis of coregulated gene sets, pathway analysis, and predicted upstream regulators, were used to analyze the DEGs (Figure 4).

Projection of the DEGs onto a zebrafish transcriptomic SOM was used to compare global changes in gene expression. As predicted, exposure to structurally similar PFAS compounds produced similar transcriptomic responses at 4 dpf (Figure S5) and 5 dpf (Figure 5A–C). Using an INfORM-based analysis, three functional groups (walktraps), consisting of 37–194 DEGs (Figure 5D–E), were identified. The sets of DEGs in walktrap 2 related to disruption of fatty acid synthesis and maintenance (Figure 5D), whereas walktrap 3 and, to a lesser extent, walktrap 4 contributed to overrepresentation of pathways involved in neurological diseases, including Huntington's, Alzheimer's, Parkinson's, and prion diseases and amyotrophic lateral sclerosis, as well as general
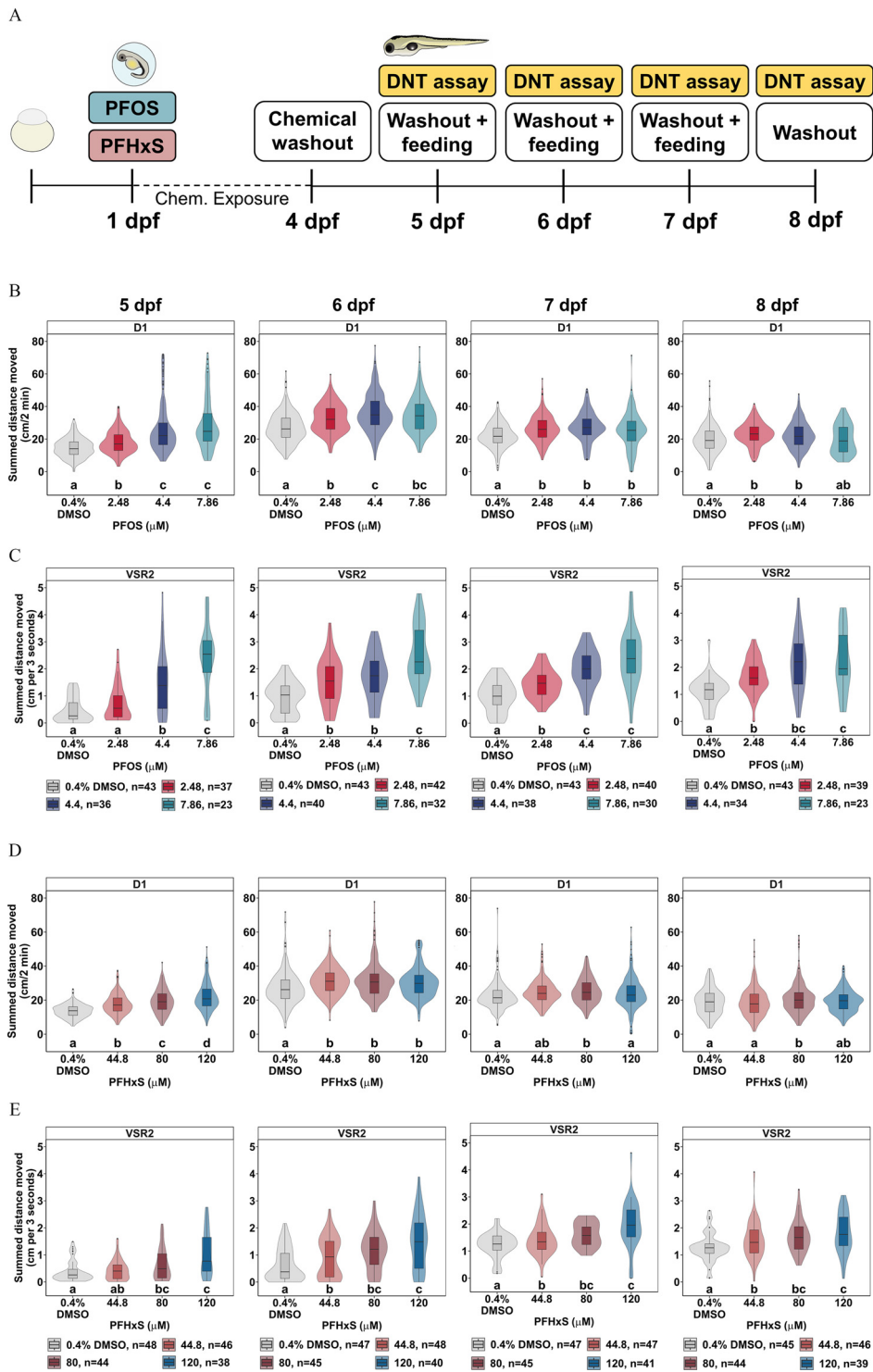
Figure 3. Washout study to characterize persistence of PFOS- or PFHxS-dependent dark-phase and VSR hyperactivity. (A) Experimental design of the washout study. (B,D) Distance moved (cm) for each larva in 2-min periods across each 10-min light phase at 13,238 lux (L1, L2) and dark phase at 0 lux (D1, D2) for behavior tests at 5–8 dpf. Data are represented as box and violin plots comprising 5 values per larva in the D1 phase. Violins around the box plots describe the kernel probability density of the underlying data. Significance was determined by Tukey-adjusted estimated marginal means following a generalized additive mixed effects model. Significant differences ($p < 0.05$) between groups are indicated by different letters. VSR data within 3 s after light–dark transition (VSR2) following developmental exposure to (C) 2.48–7.86 μM PFOS, or (E) 44.8–120 μM PFHxS are also shown for behavior tests at 5–8 dpf. Data are represented as box and violin plots that comprise 1 value per larva. Significance was determined by Tukey-adjusted estimated marginal means following a linear mixed effects model. Significant differences ($p < 0.05$) between groups are indicated by different letters. Individual box plots comprise a box that describes the IQR, a bold line that represents the median, and whiskers that indicate the calculated minimum (25th percentile $-1.5 \times$ IQR) and the calculated maximum (75th percentile $+1.5 \times$ IQR). Dots represent outliers beyond the calculated minima or maxima. Violins around the box plots describe the kernel probability density of the underlying data. Replicate numbers tested for PFOS ranged from 23 to 43 larvae (B,C) and from 38 to 48 larvae for PFHxS (D,E). Summary data can be found in Excel Tables S9–S12. Note: Chem, chemical; D, dark; DMSO, dimethyl sulfoxide; DNT, developmental neurotoxicity; dpf, days postfertilization; IQR, interquartile range; L, light; PFHxS, perfluorohexanesulfonic acid; PFOS, perfluorooctanesulfonic acid; VSR, visual startle response.
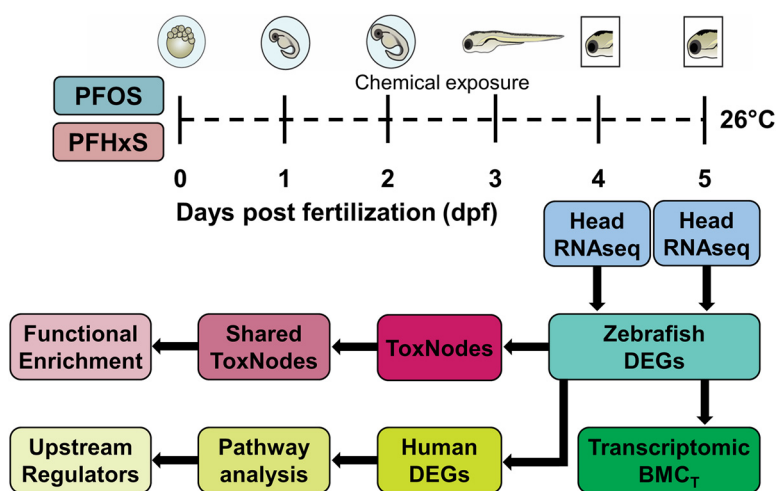
Figure 4. Experimental design for exploratory RNA-seq. Head dissections of PFOS (0.88 µM, 1.57 µM, 2.8 µM) or PFHxS (7.87 µM, 14 µM, 25.1 µM)-exposed larvae were conducted on 4–5 dpf for RNA-seq with five biological replicates per condition. Differentially expressed genes (DEGs) were used for functional enrichment analysis using ToxNodes in SOM-format, calculation of transcriptomic benchmark concentrations (BMC$_T$), and upstream regulator predictions via an Ingenuity Pathway Analysis. Note: dpf, days postfertilization; PFHxS, perfluorohexanesulfonic acid; PFOS, perfluorooctanesulfonic acid; RNA-seq, RNA sequencing; SOM, self-organizing map.

enrichment for neurodegeneration (Figure 5E). BMC–response modeling showed that larvae exposed to PFOS or PFHxS demonstrated significant differences in gene set expression at nominal concentrations that produced D1 hyperactivity in the same strain of zebrafish (Table S4). When mapped to human orthologs, upstream prediction analysis revealed that the PPARs PPARα, PPARδ, and PPARγ were potential regulators of PFOS- and PFHxS-dependent gene expression (Figure 6A). Across a suite of US EPA CompTox PPAR-specific biochemical or *in vitro* assays, there is some evidence of bioactivity following exposure to PFOS or PFHxS (Figure 6B).

Determination of ppar Essentiality for PFOS-Dependent VSR2 Hyperactivity

Based on the prediction that ppars function as potential upstream regulators of PFOS- or PFHxS-dependent VSR2 hyperactivity (Figure 6A), we hypothesized that one or more ppars are required for these chemicals to cause permanent disruption of the nervous circuit controlling the VSR2-response in developing zebrafish larvae. In zebrafish, there are two PPARα genes (*pparaa* and *pparab*), one PPARγ gene (*pparg*), and two PPARδ genes (*pparda* and *ppardb*). To test our hypothesis, we opted to knockdown all duplicated genes via the generation of *pparaa/ab*, *pparda/db*, or *pparg*-knockdown larvae (i.e., crispants) at 0 dpf (Figure 7A). To evaluate our hypothesis, we focused on PFOS because it robustly caused significant VSR2 hyperactivity in all experiments.

Larvae were injected with guide RNA sets that knocked down target gene function (set 1–8) or NC guide RNAs (i.e., NC) that do not cause mutations in the target genes (Figure 7A; Tables S1 and S2). Gene knockdown in *pparaa/ab*, *pparda/db*, or *pparg* crispants was molecularly confirmed using a qRT-PCR–based method (Figure S6). In addition, sequencing of five *pparda/db*-knockdown cut sites in F0 crispants verified the presence of indels in 90%–100% of injected individuals (Figure S7). Knockdown of *pparg* (Figure 7B), *pparaa/ab* (Figure 7C), or *pparda/db* (Figure 7D,E) did not affect baseline activity in DMSO-exposed crispants [knockdown sets (blue) vs. NC control (gray)]. In larvae exposed to 7.86 µM PFOS from 1 to 4 dpf (Figure 7B), *pparg*-knockdown failed to block or blunt chemical-dependent hyperactivity (set 1 or set 2 vs. NC crispants). In the case of *pparaa/ab*, a reduction of the

VSR2-response as compared with NC (set 3 or set 4 vs. NC) was observed; however, set 3 or set 4 crispants exposed to 7.86 µM PFOS were still hyperactive compared with unexposed NC crispants (Figure 7C). In addition, no consistent block or blunting effects on D1 hyperactivity were observed for *pparg* or *pparaa/ab* crispants exposed to PFOS (Figure S8A,B). Interestingly, PFOS-exposed crispants with *pparg*-knockdown exhibited D1 hyperactivity (Figure S8A). Molecular analysis showed successful knockdown of the *pparaa/ab* and *pparg* genes in all crispants (sets 1–4, Figure S6).

In contrast to *pparg* and *pparaa/ab*, *pparda/db*-knockdown blunted the VSR2-response to control levels following developmental exposure to 7.86 µM PFOS (Figure 7D). Successful knockdown of *ppardb* was achieved in both set 5 and set 6 crispants (Figure S6). Gene knockdown was also molecularly confirmed for *pparda* in set 6 crispants (Figure S6). The efficiency of *pparda* was not evaluated in set 5 crispants because there were no available primer sites that spanned the set 5 guide RNA cut sites. Editing of *pparda/db* genes were also verified using sequencing (Figure S7). Therefore, to confirm these data, we performed a validation study using additional *pparda* guide RNAs that were determined to lower amplicon amplification in previous experiments (Figure S6 and Table S2). In line with the data shown in Figure 7D, *pparda/db*-knockdown blunted PFOS-dependent hyperactivity to the control level (set 7, set 8 in shades of orange), relative to the negative control crispant group (NC, gray) (Figure 7E). These results suggest an interaction between *pparda/db*, PFOS, and VSR2 hyperactivity. In contrast, consistent blunting of D1 hyperactivity was not observed across experiments (Figure S8C,D).

Orthogonal Evaluation of ppard-Dependent VSR Hyperactivity in PFOS-Exposed Larvae

To provide multiple lines of evidence that *pparda/db* is required for chemical-dependent VSR2 hyperactivity, we tested whether exposure to the potent and selective *pparda/db*-antagonist GSK3787 blunted PFOS-dependent VSR2 hyperactivity. Exposure at 0 dpf to 9.25 or 27.2 µM GSK3787 alone did not affect the VSR2-response (shades of green; Figure 8). Exposure to 7.86 or 11.72 µM PFOS at 1 dpf (shades of blue) caused VSR2 hyperactivity at 5 dpf, in comparison with the DMSO control (gray) (Figure 8). In support of the *pparda/db*-knockdown experiments shown in Figure 7, larvae
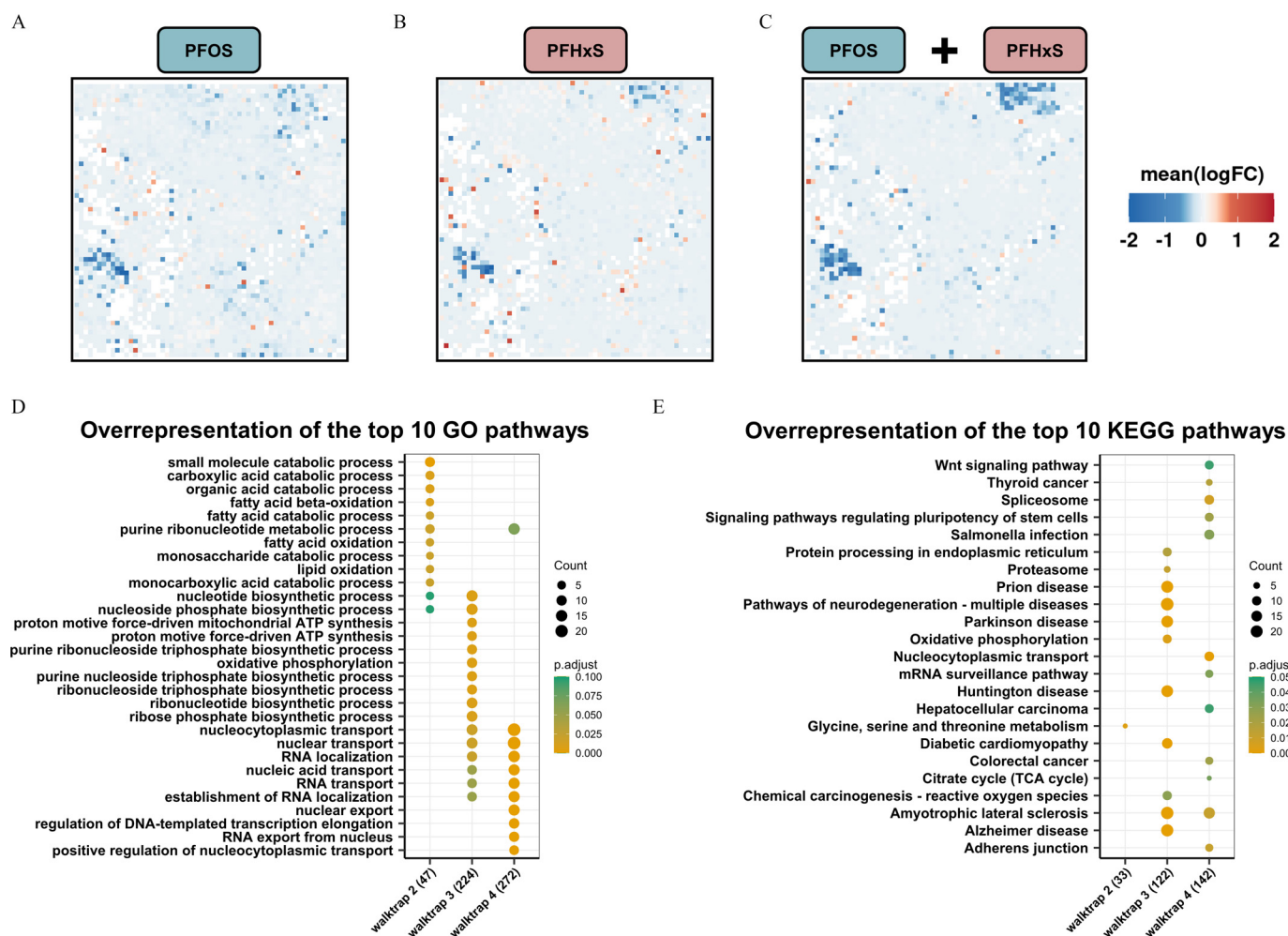
Figure 5. Global gene expression patterns and altered pathways in head tissue obtained from zebrafish developmentally exposed to PFOS or PFHxS. (A,B,C) Significantly enriched gene nodes at 5 dpf following exposure to (A) PFOS or (B) PFHxS, or (C) the combined dataset were projected onto a self-organizing map (SOM). Individual concentrations were combined for each substance and a single SOM was calculated with a treatment vs. control contrast. (See Figure S4 for 4-dpf SOMs.) Mean logarithmic fold changes (FCs) per node are shown. (D) Overrepresentation analysis of the top 10 Gene Ontology (GO) pathways based on differentially expressed genes (DEGs) identified for each functional group (i.e., walktrap) for the combined 5-dpf dataset. (E) Overrepresentation analysis of the top 10 KEGG pathways based on DEGs per walktrap. Numbers in brackets indicate the total number of genes assigned to each walktrap. The number of genes per pathway (count) and significance levels (p.adjust) are shown. Five biological replicates containing pools of 15 heads were used. RNA-seq data shown here can be found in Excel Tables S13–S18. Note: ATP, adenosine triphosphate; dpf, days postfertilization; GO, Gene Ontology; KEGG, Kyoto Encyclopedia of Genes and Genomes; PFHxS, perfluorohexanesulfonic acid; PFOS, perfluorooctanesulfonic acid; RNA-seq, RNA sequencing; TCA, tricarboxylic acid.

coexposed to 27.2 µM GSK3787 and both concentrations of PFOS blunted the VSR2 response to the control level (Figure 8).

Discussion

In this study, we investigated causal links between exposure to structurally similar alkyl sulfonic acid PFAS and behavioral effects in larval zebrafish. We used developmental and acute exposures paired with RNA-seq, gene editing, and pharmacological manipulation to reveal a novel mechanism by which exposure to PFOS caused VSR2 hyperactivity within a zebrafish DNT new approach method (NAM).

This work replicated previously observed dark-phase (D1) hyperactivity in zebrafish larvae exposed to either PFOS or PFHxS.[29] Genetic background and environmental factors, such as laboratory-specific handling and housing, have been reported to influence larval zebrafish behavior in zebrafish exposed to a range of chemicals,[65,66] including PFAS.[67] The data presented here reproduced PFOS- and PFHxS-dependent hyperactivity in the D1 period, despite study-specific differences in zebrafish strain and experimental design. This supports the concept that PFOS or PFHxS

exposures disrupt neurodevelopment via a conserved mode of action(s).

In this study, we also characterized the dark-phase hyperactivity phenotype following acute exposure to PFOS or PFHxS. We observed acute dark-phase hyperactivity for both chemicals following different exposure periods. Using a window of exposure design, we report that larvae exposed acutely to PFHxS took approximately 7 times longer to exhibit acute dark-phase hyperactivity after exposure, relative to PFOS. Across seven studies, PFHxS exposure resulted in lower bioconcentration factors, relative to PFOS (Tal and Vogs[68]). The increased bioconcentration potential of PFOS likely explains why a longer period was needed for PFHxS exposure to cause acute dark-phase hyperactivity. A recent study reported that osmoregulation modified pericardial edema (a morphological effect) in zebrafish exposed to the flame-retardant triphenyl phosphate in the presence of higher salinity.[69] Given that PFAS accumulation was elevated upon increased salinity in different marine wildlife organisms[70,71] and elevated PFAS accumulation in marine medaka was associated with salinity-induced expression of PFAS-binding proteins (i.e., OAT1
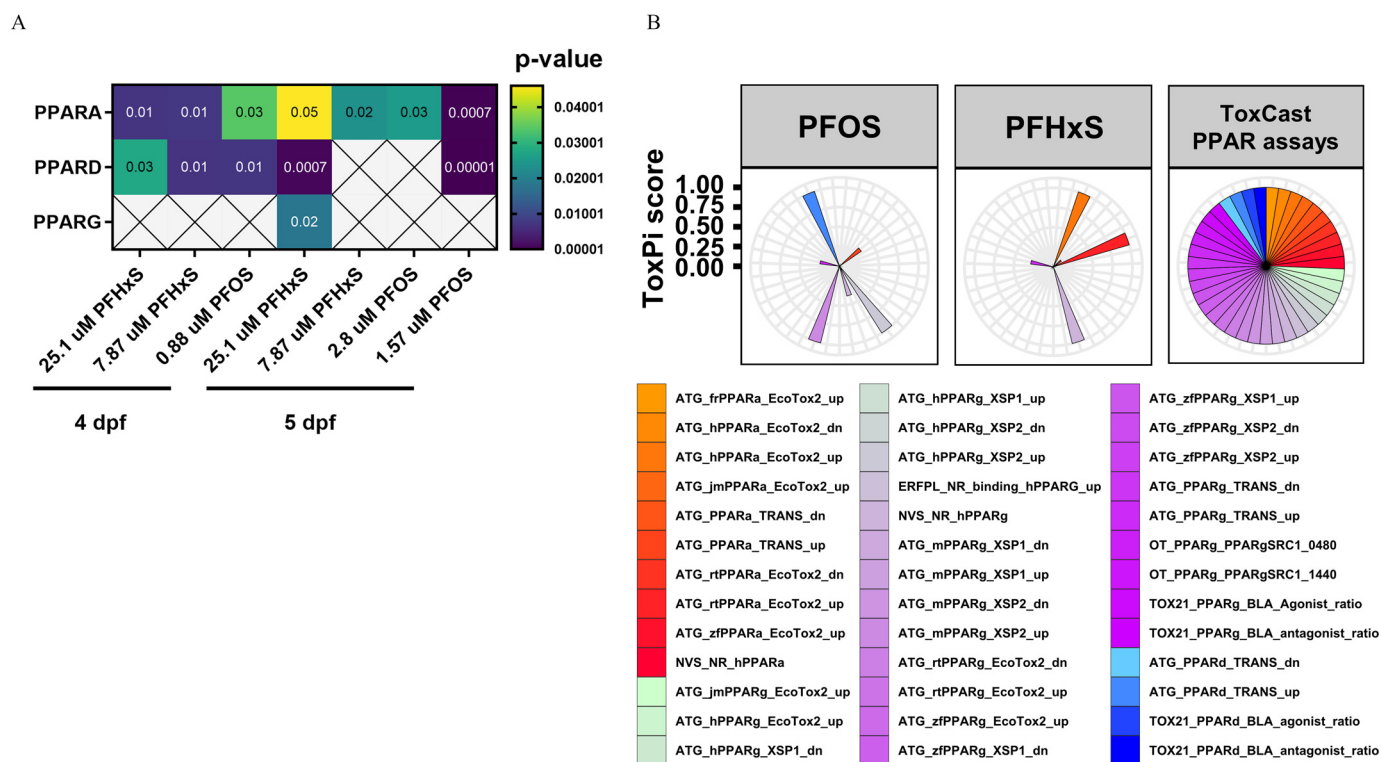
Figure 6. Predicted upstream regulators affected by developmental exposure to PFOS or PFHxS and *in vitro* potency profiles. (A) Human orthologs for zebrafish differentially expressed genes (DEGs) were analyzed by Ingenuity Pathway Analysis and predicted human PPARα, PPARδ, and PPARγ as putative upstream regulators for multiple concentrations of PFOS and PFHxS at 4–5 dpf. Significant enrichment was identified by Fisher's exact test $p < 0.05$; crosses indicate nonsignificance. Five biological replicates containing pools of 15 heads were used. (B) Visualized potency profiles of PFOS and PFHxS in US EPA CompTox (version 3.5) *in vitro* assays targeting human (h), rat (r), mouse (m), zebrafish (zf), or Japanese medaka (jm) PPARα, PPARδ, and/or PPARγ. Profiles for both chemicals were calculated based on AC_{50}-values using the ToxPi framework. Distance from the center indicates potency. All assays were weighted equally. ToxPi data can be found in Excel Table S19. Note: AC_{50}, 50% activity concentration; dpf, days postfertilization; EPA, Environmental Protection Agency; PFHxS, perfluorohexanesulfonic acid; PFOS, perfluorooctanesulfonic acid; PPAR, peroxisome proliferator-activated receptor; ToxPi, toxicity prioritization index.

and FABP),[71] future work should address whether osmoregulation influences PFAS-dependent behavioral effects. Following developmental or acute exposure, dark-phase hyperactivity was consistently observed beginning at 2.47 μM. Following developmental exposure, VSR hyperactivity was observed at 7.86 μM. These values exceed the maternal serum levels of pregnant women from the Danish National Birth Cohort[72] by roughly two orders of magnitude.

To further characterize dark-phase hyperactivity after developmental or acute exposure to PFOS or PFHxS, we conducted a depuration study and measured behavior 1–4 d after chemical removal. We observed that concentration-dependent dark-phase hyperactivity was transient. This suggests that dark-phase hyperactivity, triggered by acute exposure to PFOS or PFHxS, is mediated by direct receptor interactions rather than by permanent disruption to the development of the behavioral circuit(s) that control the stereotypic response to a dark period that follows a light period. In support of this, an *in vitro* study conducted in *Xenopus* oocytes, human induced-pluripotent stem-cell derived neuronal cocultures, and primary rat cortical cultures showed that PFOS antagonizes the most abundant receptor subunit combination of the human gamma-aminobutyric acid type A (GABA_A) receptor with a range of assay-specific lowest observed effect concentrations (LOECs; 0.1–100 μM)[73] that are in line with the concentrations tested here. The GABA_A receptor is the main inhibitory neurotransmitter in the central nervous system (CNS), and it is critical for neurodevelopment by exerting influence on long-term potentiation and synaptic plasticity.[74,75] Relative to perfluorooctanoic acid (PFOA), PFOS demonstrated higher affinity to the GABA_A receptor *in vitro*,

resulting in slower reversibility of PFOS-induced effects.[73] This is in line with our *in vivo* findings, where dark-phase hyperactivity was present 3 (PFOS) or 2 (PFHxS) d after chemical removal. In larval zebrafish, dark-phase hyperactivity has been reported following exposure to GABA_A receptor antagonists[76–78] and exposure to PFOS has been shown to directly perturb neural activity *in vivo*.[79] In addition, loss-of-function mutations in the γ2 GABA_A subunit in zebrafish was reported to induce behavioral hyperactivity.[80] Taken together, these data indicate a relationship between GABA_A receptor function and dark-phase locomotion in the light–dark transition test. Future work should explore whether the GABA_A receptor causally mediates dark-phase hyperactivity in zebrafish acutely exposed to alkyl sulfonic acid PFAS, such as PFOS and PFHxS.

In the present study, we extended the phenotypic resolution of the conventional light–dark transition test by recording data every second of the assay. This allowed us to increase the phenotypic range of zebrafish behaviors potentially disrupted by chemical exposure to include the VSR. The VSR describes a simple reflex behavior, conserved across taxa to escape from a threatening stimulus.[81] Despite the general behavior being described for nearly a century, and the introduction of the VSR as a relevant behavioral end point to understand the genetics that control vertebrate behavior,[82] it has, to our knowledge, not been considered as a relevant end point for the investigation of potential neurotoxic effects following exposure to PFAS. In the updated light–dark transition test, we measured the startle response following dark–light (VSR1) and light–dark (VSR2) transitions. After developmental exposure to either PFOS or PFHxS, we
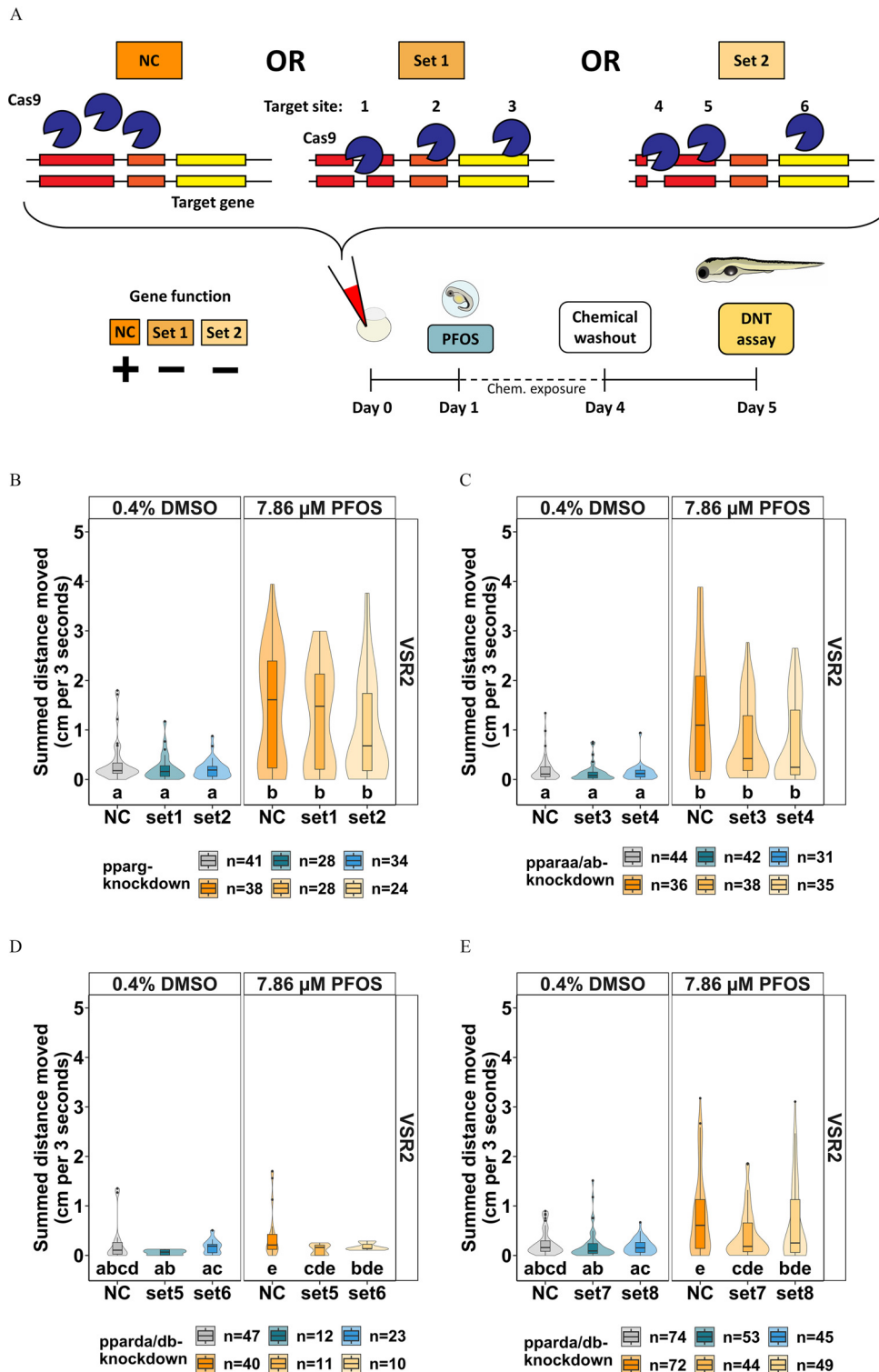
Figure 7. Knockdown study to determine the essentiality of ppar genes for VSR hyperactivity in PFOS-exposed zebrafish. (A) CRISPR/Cas9-based gene editing experimental design were embryos that experience gene knockdown (set 1 or set 2 crispants) relative to negative control crispants (NC) that did not experience gene knockdown and were subsequently exposed to 7.86 µM PFOS at 1 dpf. The chemical was removed at 4 dpf and behavior was assessed at 5 dpf. VSR within 3 s after light–dark transition (VSR2) in (B) *pparg*-knockdown, (C) *pparaa/ab*-knockdown, or (D,E) *pparda/db*-knockdown larvae exposed to 7.86 µM PFOS are shown. Data are represented as box and violin plots and comprise 1 value per larva. Significance was determined by Tukey-adjusted estimated marginal means following a linear mixed effects model. Significant differences ($p < 0.05$) between groups are indicated by different letters. Individual box plots comprise a box that describes the IQR, a bold line that represents the median, and whiskers that indicate the calculated minimum (25th percentile $−1.5\times$ IQR) and the calculated maximum (75th percentile $+1.5\times$ IQR). Dots represent outliers beyond the calculated minima or maxima. Violins around the box plots describe the kernel probability density of the underlying data. Replicate numbers were 24–41 for *pparg*-knockdown (B), 31–44 for *pparaa/ab*-knockdown (C), 10–47 for initial *pparda/db*-knockdown, and 44–75 for *pparda/db*-knockdown with revised guide sets. Summary data can be found in Excel Tables S20–S23. Note: CRISPR, Clustered Regularly Interspaced Short Palindromic Repeats; DNT, developmental neurotoxicity; dpf, days postfertilization; IQR, interquartile range; PFOS, perfluorooctanesulfonic acid; ppar, peroxisome proliferator-activated receptor; VSR, visual startle response.
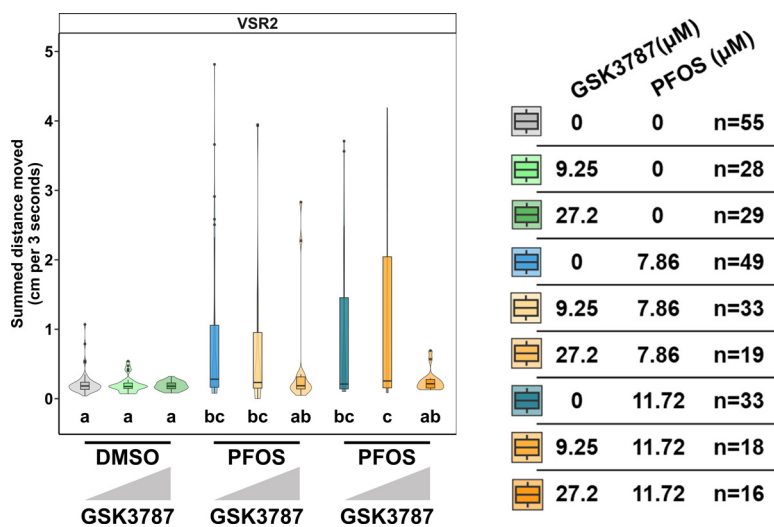
Figure 8. Coexposure of *pparda/db*-antagonist GSK3787 and PFOS. To mimic the CRISPR study design, embryos were exposed to 9.25 or 27.2 μM of the ppard antagonist GSK3787 or 0.4% DMSO at 0 dpf. At 1 dpf, embryos were exposed to 7.86 or 11.72 μM PFOS or DMSO, the chemical was removed at 4 dpf, and behavior was assessed at 5 dpf. Data shown for VSR within 3 s after light–dark transition (VSR2) are represented as box and violin plots and comprise 1 value per larva. Significance was determined by Tukey-adjusted estimated marginal means following a linear mixed effects model. Significant differences ($p < 0.05$) between groups are indicated by different letters. Individual box plots comprise a box that describes the IQR, a bold line that represents the median, and whiskers that indicate the calculated minimum (25th percentile $-1.5 \times$ IQR) and the calculated maximum (75th percentile $+1.5 \times$ IQR). Dots represent outliers beyond the calculated minima or maxima. Violins around the box plots describe the kernel probability density of the underlying data. Replicate numbers ranged from 16 to 55 larvae. Summary data can be found in Excel Table S24. Note: CRISPR, Clustered Regularly Interspaced Short Palindromic Repeats; DMSO, dimethyl sulfoxide; dpf, days postfertilization; GSK3787, ppard antagonist; IQR, interquartile range; PFOS, perfluorooctanesulfonic acid; VSR, visual startle response.

observed dark-phase and VSR2 hyperactivity. Future work should explore the possibility of a nonmonotonic concentration–response relationship in larvae developmentally exposed to PFOS or PFHxS. We initially hypothesized that dark-phase- and VSR2-hyperactivity might be dependent phenotypes (i.e., linked) because both were elevated following exposure to both test compounds. We additionally hypothesized that dark-phase and VSR2 hyperactivity might share a similar underlying mechanism in exposed larvae. Surprisingly, unlike the dark-phase hyperactivity phenotype that occurred developmentally and acutely, VSR2 hyperactivity only occurred following developmental exposure to the compounds given that acute exposure to either PFOS or PFHxS failed to cause VSR2 hyperactivity. Intriguingly, the depuration study showed that although dark-phase hyperactivity was transient and likely receptor-mediated, concentration-dependent VSR2 hyperactivity was persistent and irreversible up to 4 d following chemical removal, when the study ceased (i.e., at 8 dpf). Therefore, in contrast to dark-phase hyperactivity, we ultimately hypothesized that VSR2 hyperactivity in PFOS- or PFHxS-exposed larvae resulted from a developmental perturbation in the circuit controlling the stereotypic VSR2 response.

To shed light on underlying mechanisms that may cause developmental VSR2 hyperactivity in PFOS- or PFHxS-exposed zebrafish larvae, we used an unbiased transcriptomic strategy for hypothesis generation. DEGs were projected onto a zebrafish SOM.[56] This approach integrates and aggregates time- and concentration-resolved toxicogenomic data to generate comparable toxicogenomic fingerprints.[56] Our analysis showed that exposure to structurally similar PFOS or PFHxS produced similar global changes in transcriptomics. Although the SOM analysis revealed similar clusters of coregulated genes, their underlying functions are not clear. We used an INfORM-based analysis to better understand potential functions associated with differentially expressed gene sets (i.e., walktraps).[58] We identified functional gene clusters related to pathways controlling different stages of neurodevelopment. From a global perspective, similar gene clusters in larval head tissue were dysregulated following

developmental exposure to PFOS or PFHxS, further indicating that these structurally similar chemicals provoke the same behavior phenotypes via a potential shared mechanism. It also supports previous work showing that exposure to similar concentrations of PFOS, disrupted neurodevelopmental pathways related to axonal deformation, neuroinflammatory stimulation, and dysregulation of calcium-signaling pathways.[83] However, it remains unclear whether gene expression changes and pathway-level perturbations are causative or simply associated with compound exposure.

BMC–response modeling is increasingly used to assess data generated using NAMs as it allows for direct comparisons of effect concentrations across assays and laboratories.[84,85] BMC modeling has also been widely applied to transcriptomic data.[86–88] In our study, BMC modeling showed significant differences in gene set expression, before the onset of hyperactivity (Table S4 and Gaballah et al.[29]). We therefore hypothesized that, rather than describe putative dysregulated signaling pathways, transcriptomic data could be used to identify an underlying mechanism(s) by which PFOS or PFHxS exposure caused VSR2 hyperactivity. We identified *ppars* as predicted upstream regulators that might explain the observed gene expression differences and related VSR2 hyperactivity phenotype. PPARs have a wide variety of vital roles in fatty acid transportation and catabolism, glucose metabolism, adipogenesis, thermogenesis, cholesterol transportation and synthesis, and anti-inflammatory response.[89] In the developing nervous system of rats, PPARα and PPARδ mRNAs were omnipresent in different brain regions, whereas PPARγ levels were low.[90] In zebrafish, *in situ* hybridization studies showed that orthologous genes, including *pparaa/ab*, *pparg*, and *pparda/db*, are expressed throughout the developing nervous system.[91,92] In line with a previous study conducted in whole larvae,[93] we identified PPARs as putative upstream regulators at both time points, following exposure to multiple concentrations of PFOS or PFHxS. PPARs are routinely associated with exposure to a wide range of PFAS, including PFOS and PFHxS, in mammalian transcriptomic

studies[94,95] and in *in vitro* high-throughput signaling assays[96] and the liver is considered to be a major target of PFAS.[97] Despite this understanding, their potential role in chemical-dependent DNT has yet to be described.

Adverse outcome pathways (AOPs) serve as a conceptual basis to link chemical exposures, key events, and adverse outcomes that are of potential regulatory relevance.[98] Key events can be represented by a series of NAMs and assembled into testing batteries that can be used to reduce, replace, or refine animal tests as part of an Integrated Approach to Testing and Assessment (IATA).[99] AOPs are assembled based on a weight-of-evidence approach showing biological links between key events and adverse outcomes (i.e., biological plausibility) and associated toxicological data supporting such links.[98] AOP weight of evidence can also be increased if effects are observed in multiple species or effect patterns are consistent for structurally similar compounds.[100] One underused strategy to build confidence in NAMs for risk assessment is to demonstrate key event essentiality or demonstration that an event must occur for downstream effects to manifest.[101]

We used CRISPR/Cas9 gene editing to causally investigate whether *pparaa/ab*, *pparg*, or *pparda/db* were required for PFOS exposure to cause VSR2 hyperactivity. In contrast to the transient nature of morpholino knockdowns,[102] CRISPR/Cas9 knockdown results in a stable loss of gene function across successive cells within an edited cell lineage in F0 crispants.[31] We adapted a previously published strategy to generate F0 knockdown zebrafish larvae[31] to generate diverse null alleles via the use of guide RNAs that targeted three different cut sites on different exons (wherever possible) on the same target gene to consistently induce gene loss of function. Multiplexing guide RNAs against the same target gene was recommended[31] to decrease the likelihood that compensatory mechanisms allow for the production of functional proteins in F0 crispants.[103] It has been reported that diversity in null-allele (i.e., knockout) organisms experiencing gene knockout may produce different phenotypes.[104,105] In contrast, genetically diverse F0 knockdown animals are posited to provide a reproducible and robust outcome caused by the absence of the functional protein.[31] As a foundational strategy to ensure data reproducibility, we also designed a second set of guideRNAs targeting three different sites in the same target gene. Here, we only report concordant behavior effects, across both CRISPR sets, as a positive result. We therefore exclude the possibility of discordant effects that could be explained by off-target knockdown. This strategy builds confidence in resulting data as it *a*) reduces the possibility of confounding off-target effects that are unlikely to be present in both sets of disparate gRNAs that target the same gene, and *b*) should provoke similar outcomes across all paired sets. This robust design was hypothesized to reveal the same mechanistic data for both sets of *ppar* crispants evaluated in each experiment.

In line with phenotyping experiments showing acute and transient dark-phase hyperactivity, *pparaa/ab, pparda/da*, and *pparg* were not required for PFOS exposure to evoke dark-phase hyperactivity. Our results also showed that *pparaa/ab* or *pparg* were dispensable for PFOS exposure to cause developmental perturbation of the behavior circuit that controls the stereotypic VSR2 hyperactivity response. In contrast, based on multiple lines of evidence, we propose that there is a key event relationship that causally links *pparda/db* to the downstream VSR2 hyperactivity key event in a novel AOP for DNT. Key event essentiality was demonstrated with both sets of crispants that experienced *pparda/db*-knockdown and following exposure to PFOS and this result was confirmed in coexposure experiments using a *pparda/db*-antagonist. We observed concordant results in acute and developmental exposure experiments, the depuration study, and the transcriptomic experiments in zebrafish exposed to PFOS or PFHxS.

Future work should evaluate the hypothesis that PFHxS and other structurally similar alkyl sulfonic acid PFAS cause VSR hyperactivity via a *pparda/db*-dependent mechanism.

In mice, PPARδ is the most abundant receptor subtype in the CNS,[106] where it is specifically and highly expressed in medium spiny neurons in the striatum, an area of the brain involved with motor function.[107] In support of a role of PPARδ in locomotor circuits, expression of dominant-negative PPARδ in the mouse CNS was sufficient to induce motor dysfunction.[108] Collectively, this supports a role for *ppard* in vertebrate locomotion and additionally suggests that *ppard* may be involved in the development of the VSR in zebrafish. Although more information on the number and cellular distribution of this receptor across species is needed, we submit that these findings may be relevant for humans, as the human PPARδ and zebrafish pparda/db proteins share 71%–73% similarity, demonstrating high conservation between protein structure and putative function.[109]

DNT studies are typically assessed in Organisation for Economic Co-operation and Development (OECD) or US EPA guideline studies.[110,111] These guidelines are based on rodent tests that are time consuming, costly,[112] and ethically questionable such that DNT hazard information is only available for 110–140 compounds of an estimated ∼350,000 registered chemicals and mixtures.[113–115] A next-generation high-throughput *in vitro* DNT test battery has been assessed by the European Food Safety Authority, conducted in human-derived stem-cell models, and captures a range of neurodevelopmentally relevant cellular events.[116] From a functional perspective, the integrated battery[117] also includes functional neuronal activity measurements captured on microelectrode arrays.[118,119] However, these *in vitro* assays, by design, are unable to provide direct analogs for OECD TG 426 test end points including motor activity, motor and sensory function, learning and memory, brain morphometry, and histopathology analyses.[110] The expanded light–dark transition test reported here includes end points for motor activity and motor and sensory function (i.e., VSR). When combined with zebrafish-based NAMs for learning and memory,[120] and automated brain morphometrics,[121] which can be evaluated in the same larvae post behavior, we submit that larval zebrafish behavior tests have the potential to add value to 3R-compliant DNT testing strategies to ultimately identify chemicals that pose a threat to the developing nervous systems in humans and other animals.

Acknowledgments

References

1. Williams AJ, Gaines LGT, Grulke CM, Lowe CN, Sinclair GFB, Samano V, et al. 2022. Assembly and curation of lists of per- and polyfluoroalkyl substances

(PFAS) to support environmental science research. Front Environ Sci 10:1–13, PMID: 35936994, https://doi.org/10.3389/fenvs.2022.850019.

2. Banks RE, Smart BE, Tatlow J. 2013. *Organofluorine Chemistry: Principles and Commercial Applications*. New York, NY: Springer Science & Business Media.

3. Kissa E. 2001. *Fluorinated Surfactants and Repellents*. 2nd ed. New York, NY: Marcel Dekker.

4. Lindstrom AB, Strynar MJ, Libelo EL. 2011. Polyfluorinated compounds: past, present, and future. Environ Sci Technol 45(19):7954–7961, PMID: 21866930, https://doi.org/10.1021/es2011622.

5. Schultz MM, Barofsky DF, Field JA. 2003. Fluorinated alkyl surfactants. Environ Eng Sci 20(5):487–501, https://doi.org/10.1089/109287503768335959.

6. Gawor A, Shunthirasingham C, Hayward SJ, Lei YD, Gouin T, Mmereki BT, et al. 2014. Neutral polyfluoroalkyl substances in the global atmosphere. Environ Sci Process Impacts 16(3):404–413, PMID: 24232015, https://doi.org/10.1039/c3em00499f.

7. Rankin K, Mabury SA, Jenkins TM, Washington JW. 2016. A North American and global survey of perfluoroalkyl substances in surface soils: distribution patterns and mode of occurrence. Chemosphere 161:333–341, PMID: 27441993, https://doi.org/10.1016/j.chemosphere.2016.06.109.

8. Pan Y, Zhang H, Cui Q, Sheng N, Yeung LWY, Sun Y, et al. 2018. Worldwide distribution of novel perfluoroether carboxylic and sulfonic acids in surface water. Environ Sci Technol 52(14):7621–7629, PMID: 29749740, https://doi.org/10.1021/acs.est.8b00829.

9. Ahrens L, Bundschuh M. 2014. Fate and effects of poly- and perfluoroalkyl substances in the aquatic environment: a review. Environ Toxicol Chem 33(9):1921–1929, PMID: 24924660, https://doi.org/10.1002/etc.2663.

10. Escoruela J, Garreta E, Ramos R, González-Solís J, Lacorte S. 2018. Occurrence of *per*- and polyfluoroalkyl substances in *Calonectris* shearwaters breeding along the Mediterranean and Atlantic colonies. Mar Pollut Bull 131(pt A):335–340, PMID: 29886955, https://doi.org/10.1016/j.marpolbul.2018.04.032.

11. Vestergren R, Cousins IT. 2009. Tracking the pathways of human exposure to perfluorocarboxylates. Environ Sci Technol 43(15):5565–5575, PMID: 19731646, https://doi.org/10.1021/es900228k.

12. Daly ER, Chan BP, Talbot EA, Nassif J, Bean C, Cavallo SJ, et al. 2018. Per- and polyfluoroalkyl substance (PFAS) exposure assessment in a community exposed to contaminated drinking water, New Hampshire, 2015. Int J Hyg Environ Health 221(3):569–577, PMID: 29514764, https://doi.org/10.1016/j.ijheh.2018.02.007.

13. Jain RB. 2018. Time trends over 2003–2014 in the concentrations of selected perfluoroalkyl substances among US adults aged ≥20 years: interpretational issues. Sci Total Environ 645:946–957, PMID: 30248883, https://doi.org/10.1016/j.scitotenv.2018.07.198.

14. Ramhøj L, Hass U, Boberg J, Scholze M, Christiansen S, Nielsen F, et al. 2018. Perfluorohexane sulfonate (PFHxS) and a mixture of endocrine disrupters reduce thyroxine levels and cause antiandrogenic effects in rats. Toxicol Sci 163(2):579–591, PMID: 29518214, https://doi.org/10.1093/toxsci/kfy055.

15. Zeng Z, Song B, Xiao R, Zeng G, Gong J, Chen M, et al. 2019. Assessing the human health risks of perfluorooctane sulfonate by in vivo and in vitro studies. Environ Int 126:598–610, PMID: 30856447, https://doi.org/10.1016/j.envint.2019.03.002.

16. US EPA (US Environmental Protection Agency). 2023. *Proposed PFAS National Primary Drinking Water Regulation*. Washington, DC: US EPA. https://www.epa.gov/sdwa/proposed-pfas-national-primary-drinking-water-regulation [accessed 26 June 2024].

17. Cao Y, Ng C. 2021. Absorption, distribution, and toxicity of per- and polyfluoroalkyl substances (PFAS) in the brain: a review. Environ Sci Processes Impacts 23(11):1623–1640, PMID: 34533150, https://doi.org/10.1039/D1EM00228G.

18. Stein CR, Savitz DA. 2011. Serum perfluorinated compound concentration and attention deficit/hyperactivity disorder in children 5–18 years of age. Environ Health Perspect 119(10):1466–1471, PMID: 21665566, https://doi.org/10.1289/ehp.1003538.

19. Stein CR, Savitz DA, Bellinger DC. 2014. Perfluorooctanoate exposure in a highly exposed community and parent and teacher reports of behaviour in 6–12-year-old children. Paediatr Perinat Epidemiol 28(2):146–156, PMID: 24320613, https://doi.org/10.1111/ppe.12097.

20. Lien GW, Huang CC, Shiu JS, Chen MH, Hsieh WS, Guo YL, et al. 2016. Perfluoroalkyl substances in cord blood and attention deficit/hyperactivity disorder symptoms in seven-year-old children. Chemosphere 156:118–127, PMID: 27174824, https://doi.org/10.1016/j.chemosphere.2016.04.102.

21. Lenters V, Iszatt N, Forns J, Čechová E, Kočan A, Legler J, et al. 2019. Early-life exposure to persistent organic pollutants (OCPs, PBDEs, PCBs, PFASs) and attention-deficit/hyperactivity disorder: a multi-pollutant analysis of a Norwegian birth cohort. Environ Int 125:33–42, PMID: 30703609, https://doi.org/10.1016/j.envint.2019.01.020.

22. Ulhaq M, Orn S, Carlsson G, Morrison DA, Norrgren L. 2013. Locomotor behavior in zebrafish (*Danio rerio*) larvae exposed to perfluoroalkyl acids. Aquat Toxicol 144–145:332–340, PMID: 24215719, https://doi.org/10.1016/j.aquatox.2013.10.021.

23. Jantzen CE, Annunziato KA, Bugel SM, Cooper KR. 2016. PFOS, PFNA, and PFOA sub-lethal exposure to embryonic zebrafish have different toxicity profiles in terms of morphometrics, behavior and gene expression. Aquat Toxicol 175:160–170, PMID: 27058923, https://doi.org/10.1016/j.aquatox.2016.03.026.

24. Rericha Y, Cao D, Truong L, Simonich M, Field JA, Tanguay RL. 2021. Behavior effects of structurally diverse per-and polyfluoroalkyl substances in zebrafish. Chem Res Toxicol 34(6):1409–1416, PMID: 34018735, https://doi.org/10.1021/acs.chemrestox.1c00101.

25. Wasel O, Thompson KM, Gao Y, Godfrey AE, Gao J, Mahapatra CT, et al. 2021. Comparison of zebrafish in vitro and in vivo developmental toxicity assessments of perfluoroalkyl acids (PFAAs). J Toxicol Environ Health A 84(3):125–136, PMID: 33143551, https://doi.org/10.1080/15287394.2020.1842272.

26. Truong L, Rericha Y, Thunga P, Marvel S, Wallis D, Simonich MT, et al. 2022. Systematic developmental toxicity assessment of a structurally diverse library of PFAS in zebrafish. J Hazard Mater 431:128615, PMID: 35263707, https://doi.org/10.1016/j.jhazmat.2022.128615.

27. Vogs C, Johanson G, Näslund M, Wulff S, Sjödin M, Hellstrandh M, et al. 2019. Toxicokinetics of perfluorinated alkyl acids influences their toxic potency in the zebrafish embryo (*Danio rerio*). Environ Sci Technol 53(7):3898–3907, PMID: 30844262, https://doi.org/10.1021/acs.est.8b07188.

28. Menger F, Pohl J, Ahrens L, Carlsson G, Örn S. 2020. Behavioural effects and bio-concentration of per-and polyfluoroalkyl substances (PFASs) in zebrafish (*Danio rerio*) embryos. Chemosphere 245:125573, PMID: 31877453, https://doi.org/10.1016/j.chemosphere.2019.125573.

29. Gaballah S, Swank A, Sobus JR, Howey XM, Schmid J, Catron T, et al. 2020. Evaluation of developmental toxicity, developmental neurotoxicity, and tissue dose in zebrafish exposed to GenX and other PFAS. Environ Health Perspect 128(4):047005, PMID: 32271623, https://doi.org/10.1289/EHP5843.

30. Sorlien EL, Witucki MA, Ogas J. 2018. Efficient production and identification of CRISPR/Cas9-generated gene knockouts in the model system *Danio rerio*. J Vis Exp 138:e56969, PMID: 30222157, https://doi.org/10.3791/56969.

31. Kroll F, Powell GT, Ghosh M, Gestri G, Antinucci P, Hearn TJ, et al. 2021. A simple and effective F0 knockout method for rapid screening of behaviour and other complex phenotypes. elife 10:e59683, PMID: 33416493, https://doi.org/10.7554/eLife.59683.

32. Kimmel CB, Ballard WW, Kimmel SR, Ullmann B, Schilling TF. 1995. Stages of embryonic development of the zebrafish. Dev Dyn 203(3):253–310, PMID: 8589427, https://doi.org/10.1002/aja.1002030302.

33. Wood SN. 2017. *Generalized Additive Models: An Introduction with R*. 2nd ed. New York, NY: Chapman and Hall/CRC.

34. Lenth RV. 2021. emmeans: estimated marginal means, aka least-squares means. https://cran.r-project.org/web/packages/emmeans/index.html [accessed 26 June 2024].

35. Wickham H. 2017. reshape2: flexibly reshape data: a reboot of the reshape package. https://cran.r-project.org/web/packages/reshape2/index.html [accessed 26 June 2024].

36. Wickham H, Chang W, Henry L, Takahashi K, Wilke C, Woo K, et al. 2022. ggplot2: create elegant data visualisations using the grammar of graphics. https://search.r-project.org/CRAN/refmans/ggplot2/html/ggplot2-package.html [accessed 26 June 2024].

37. Fox J, Weisberg S, Price B. 2021. car: companion to applied regression. https://cran.r-project.org/web/packages/car/index.html [accessed 26 June 2024].

38. Wickham H, François R, Henry L, Müller K. 2021. dplyr: a grammar of data manipulation. https://cran.r-project.org/web/packages/dplyr/index.html [accessed 26 June 2024].

39. Barrett T, Dowle M, Srinivasan A, Gorecki J, Chirico M, Hocking T. 2021. *data.table: Extension of 'data.frame'*. https://r-datatable.com [accessed 26 June 2024].

40. Schauberger P, Walker A. 2021. openxlsx: read, write and edit xlsx files. https://cran.r-project.org/web/packages/openxlsx/index.html [accessed 26 June 2024].

41. Graves S, Piepho HP, Selzer L. 2019. multcompView: visualizations of paired comparisons. https://cran.r-project.org/web/packages/multcompView/index.html [accessed 26 June 2024].

42. Bates D, Mächler M, Bolker B, Walker S. 2015. Fitting linear mixed-effects models using lme4. J Stat Soft 67(1):1–48, https://doi.org/10.18637/jss.v067.i01.

43. Wickham H, Averick M, Bryan J, Chang W, D'Agostino McGowan L, François R, et al. 2019. Welcome to the tidyverse. J Open Source Softw 4(43):1686, https://doi.org/10.21105/joss.01686.

44. Meeker ND, Hutchinson SA, Ho L, Trede NS. 2007. Method for isolation of PCR-ready genomic DNA from zebrafish tissues. Biotechniques 43(5):610–614, PMID: 18072590, https://doi.org/10.2144/000112619.

45. Yu C, Zhang Y, Yao S, Wei Y. 2014. A PCR based protocol for detecting indel mutations induced by TALENs and CRISPR/Cas9 in zebrafish. PLoS One 9(6):e98282, PMID: 24901507, https://doi.org/10.1371/journal.pone.0098282.

46. Untergasser A, Cutcutache I, Koressaar T, Ye J, Faircloth BC, Remm M, et al. 2012. Primer3—new capabilities and interfaces. Nucleic Acids Res 40(15): e115, PMID: 22730293, https://doi.org/10.1093/nar/gks596.

47. Bodenhofer U, Bonatesta E, Horejš-Kainrath C, Hochreiter S. 2015. Msa: an R package for multiple sequence alignment. Bioinformatics 31(24):3997–3999, PMID: 26315911, https://doi.org/10.1093/bioinformatics/btv494.

48. Larkin MA, Blackshields G, Brown NP, Chenna R, McGettigan PA, McWilliam H, et al. 2007. Clustal W and clustal X version 2.0. Bioinformatics 23(21):2947–2948, PMID: 17846036, https://doi.org/10.1093/bioinformatics/btm404.

49. Raghavan V. 2022. seqvisr (v0.2.7). Zenodo. https://doi.org/10.5281/zenodo.6583981.

50. Tal T, Kilty C, Smith A, LaLone C, Kennedy B, Tennant A, et al. 2017. Screening for angiogenic inhibitors in zebrafish to evaluate a predictive model for developmental vascular toxicity. Reprod Toxicol 70:70–81, PMID: 28007540, https://doi.org/10.1016/j.reprotox.2016.12.004.

51. Phillips JR, Svoboda DL, Tandon A, Patel S, Sedykh A, Mav D, et al. 2019. BMDExpress 2: enhanced transcriptomic dose-response analysis workflow. Bioinformatics 35(10):1780–1782, PMID: 30329029, https://doi.org/10.1093/bioinformatics/bty878.

52. National Toxicology Program. 2018. *NTP Research Report on National Toxicology Program Approach to Genomic Dose-Response Modeling.* Research Report 5. Durham, NC: National Toxicology Program.

53. Thomas RS, Allen BC, Nong A, Yang L, Bermudez E, Clewell HJ III, et al. 2007. A method to integrate benchmark dose estimates with genomic data to assess the functional effects of chemical exposure. Toxicol Sci 98(1):240–248, PMID: 17449896, https://doi.org/10.1093/toxsci/kfm092.

54. Posada D, Buckley TR. 2004. Model selection and model averaging in phylogenetics: advantages of Akaike information criterion and Bayesian approaches over likelihood ratio tests. Syst Biol 53(5):793–808, PMID: 15545256, https://doi.org/10.1080/10635150490522304.

55. US EPA. 2012. *Benchmark Dose Technical Guidance.* EPA/100/R-12/001. Washington, DC: US EPA.

56. Schüttler A, Altenburger R, Ammar M, Bader-Blukott M, Jakobs G, Knapp J, et al. 2019. Map and model—moving from observation to prediction in toxicogenomics. Gigascience 8(6):giz057, PMID: 31140561, https://doi.org/10.1093/gigascience/giz057.

57. Ritchie ME, Phipson B, Wu D, Hu Y, Law CW, Shi W, et al. 2015. *limma* powers differential expression analyses for RNA-sequencing and microarray studies. Nucleic Acids Res 43(7):e47, PMID: 25605792, https://doi.org/10.1093/nar/gkv007.

58. Marwah VS, Kinaret PAS, Serra A, Scala G, Lauerma A, Fortino V, et al. 2018. INfORM: inference of NetwOrk response modules. Bioinformatics 34(12):2136–2138, PMID: 29425308, https://doi.org/10.1093/bioinformatics/bty063.

59. Seal RL, Braschi B, Gray K, Jones TEM, Tweedie S, Haim-Vilmovsky L, et al. 2023. Genenames.org: the HGNC resources in 2023. Nucleic Acids Res 51(D1): D1003–D1009, PMID: 36243972, https://doi.org/10.1093/nar/gkac888.

60. Kanehisa M, Furumichi M, Sato Y, Kawashima M, Ishiguro-Watanabe M. 2023. KEGG for taxonomy-based analysis of pathways and genomes. Nucleic Acids Res 51(D1):D587–D592, PMID: 36300620, https://doi.org/10.1093/nar/gkac963.

61. Ashburner M, Ball CA, Blake JA, Botstein D, Butler H, Cherry JM, et al. 2000. Gene ontology: tool for the unification of biology. The Gene Ontology Consortium. Nat Genet 25(1):25–29, PMID: 10802651, https://doi.org/10.1038/75556.

62. Gene Ontology Consortium. 2021. The Gene Ontology resource: enriching a GOld mine. Nucleic Acids Res 49(D1):D325–D334, PMID: 33290552, https://doi.org/10.1093/nar/gkaa1113.

63. Feshuk M, Brown J, Davidson-Fritz S, Friedman K. 2022. *Invitrodb version 3.5 release.* Washington, DC: US EPA.

64. Marvel SW, To K, Grimm FA, Wright FA, Rusyn I, Reif DM. 2018. ToxPi Graphical User Interface 2.0: dynamic exploration, visualization, and sharing of integrated data models. BMC Bioinformatics 19(1):80, PMID: 29506467, https://doi.org/10.1186/s12859-018-2089-2.

65. Wallis DJ, Truong L, La Du J, Tanguay RL, Reif DM. 2021. Uncovering evidence for endocrine-disrupting chemicals that elicit differential susceptibility through gene-environment interactions. Toxics 9(4):77, PMID: 33917455, https://doi.org/10.3390/toxics9040077.

66. Balik-Meisner M, Truong L, Scholl EH, La Du JK, Tanguay RL, Reif DM. 2018. Elucidating gene-by-environment interactions associated with differential susceptibility to chemical exposure. Environ Health Perspect 126(6):067010, PMID: 29968567, https://doi.org/10.1289/EHP2662.

67. Wallis DJ, La Du J, Thunga P, Elson D, Truong L, Kolluri SK, et al. 2022. Leveraging a high-throughput screening method to identify mechanisms of individual susceptibility differences in a genetically diverse zebrafish model. Front Toxicol 4:846221, PMID: 35573279, https://doi.org/10.3389/ftox.2022.846221.

68. Tal T, Vogs C. 2021. Invited perspective: PFAS bioconcentration and biotransformation in early life stage zebrafish and its implications for human health protection. Environ Health Perspect 129(7):071304, PMID: 34288732, https://doi.org/10.1289/EHP9625.

69. Wiegand J, Avila-Barnard S, Nemarugommula C, Lyons D, Zhang S, Stapleton HM, et al. 2023. Triphenyl phosphate-induced pericardial edema in zebrafish embryos is dependent on the ionic strength of exposure media. Environ Int 172:107757, PMID: 36680802, https://doi.org/10.1016/j.envint.2023.107757.

70. Jeon J, Kannan K, Lim HK, Moon HB, Ra JS, Kim SD. 2010. Bioaccumulation of perfluorochemicals in Pacific oyster under different salinity gradients. Environ Sci Technol 44(7):2695–2701, PMID: 20230022, https://doi.org/10.1021/es100151r.

71. Avellán-Llaguno RD, Liu X, Liu L, Dong S, Huang Q. 2020. Elevated bioaccumulation of PFAAs in *Oryzias melastigma* following the increase of salinity is associated with the up-regulated expression of PFAA-binding proteins. Sci Total Environ 725:138336, PMID: 32298882, https://doi.org/10.1016/j.scitotenv.2020.138336.

72. Fei C, McLaughlin JK, Tarone RE, Olsen J. 2007. Perfluorinated chemicals and fetal growth: a study within the Danish National Birth Cohort. Environ Health Perspect 115(11):1677–1682, PMID: 18008003, https://doi.org/10.1289/ehp.10506.

73. Tukker AM, Bouwman LMS, van Kleef RGDM, Hendriks HS, Legler J, Westerink RHS. 2020. Perfluorooctane sulfonate (PFOS) and perfluorooctanoate (PFOA) acutely affect human $\alpha_1\beta_2\gamma_{2L}$ GABA$_A$ receptor and spontaneous neuronal network function *in vitro*. Sci Rep 10(1):5311, PMID: 32210279, https://doi.org/10.1038/s41598-020-62152-2.

74. Represa A, Ben-Ari Y. 2005. Trophic actions of GABA on neuronal development. Trends Neurosci 28(6):278–283, PMID: 15927682, https://doi.org/10.1016/j.tins.2005.03.010.

75. Fujii S, Jia Y, Yang A, Sumikawa K. 2000. Nicotine reverses GABAergic inhibition of long-term potentiation induction in the hippocampal CA1 region. Brain Res 863(1–2):259–265, PMID: 10773216, https://doi.org/10.1016/s0006-8993(00)02119-3.

76. Baraban SC, Taylor MR, Castro PA, Baier H. 2005. Pentylenetetrazole induced changes in zebrafish behavior, neural activity and c-fos expression. Neuroscience 131(3):759–768, PMID: 15730879, https://doi.org/10.1016/j.neuroscience.2004.11.031.

77. Baxendale S, Holdsworth CJ, Meza Santoscoy PL, Harrison MRM, Fox J, Parkin CA, et al. 2012. Identification of compounds with anti-convulsant properties in a zebrafish model of epileptic seizures. Dis Model Mech 5(6):773–784, PMID: 22730455, https://doi.org/10.1242/dmm.010090.

78. Cho SJ, Park E, Baker A, Reid AY. 2020. Age bias in zebrafish models of epilepsy: what can we learn from old fish? Front Cell Dev Biol 8:573303, PMID: 33015065, https://doi.org/10.3389/fcell.2020.573303.

79. Paquette SE, Martin NR, Rodd A, Manz KE, Camarillo M, Allen E, et al. 2022. Dysregulation of neural activity and microglia function following exposure to the global environmental contaminant perfluorooctane sulfonate (PFOS). bioRxiv. Preprint posted online 3 October 2022, https://doi.org/10.1101/2022.09.30.510316.

80. Liao M, Kundap U, Rosch RE, Burrows DRW, Meyer MP, Ouled Amar Bencheikh B, et al. 2019. Targeted knockout of GABA-A receptor gamma 2 subunit provokes transient light-induced reflex seizures in zebrafish larvae. Dis Model Mech 12(11):dmm040782, PMID: 31582559, https://doi.org/10.1242/dmm.040782.

81. Landis C, Hunt W. 1939. *The Startle Pattern.* New York, NY: Farrar & Rinehart.

82. Burgess HA, Granato M. 2007. Modulation of locomotor activity in larval zebrafish during light adaptation. J Exp Biol 210(pt 14):2526–2539, PMID: 17601957, https://doi.org/10.1242/jeb.003939.

83. Lee H, Sung EJ, Seo S, Min EK, Lee JY, Shim I, et al. 2021. Integrated multiomics analysis reveals the underlying molecular mechanism for developmental neurotoxicity of perfluorooctanesulfonic acid in zebrafish. Environ Int 157:106802, PMID: 34358914, https://doi.org/10.1016/j.envint.2021.106802.

84. Behl M, Hsieh JH, Shafer TJ, Mundy WR, Rice JR, Boyd WA, et al. 2015. Use of alternative assays to identify and prioritize organophosphorus flame retardants for potential developmental and neurotoxicity. Neurotoxicol Teratol 52(pt B):181–193, PMID: 26386178, https://doi.org/10.1016/j.ntt.2015.09.003.

85. Hsieh JH, Ryan K, Sedykh A, Lin JA, Shapiro AJ, Parham F, et al. 2019. Application of benchmark concentration (BMC) analysis on zebrafish data: a new perspective for quantifying toxicity in alternative animal models. Toxicol Sci 167(1):92–104, PMID: 30321397, https://doi.org/10.1093/toxsci/kfy258.

86. Farmahin R, Williams A, Kuo B, Chepelev NL, Thomas RS, Barton-Maclaren TS, et al. 2017. Recommended approaches in the application of toxicogenomics to derive points of departure for chemical risk assessment. Arch Toxicol 91(5):2045–2065, PMID: 27928627, https://doi.org/10.1007/s00204-016-1886-5.

87. Thomas RS, Clewell HJ III, Allen BC, Yang L, Healy E, Andersen ME. 2012. Integrating pathway-based transcriptomic data into quantitative chemical risk assessment: a five chemical case study. Mutat Res 746(2):135–143, PMID: 22305970, https://doi.org/10.1016/j.mrgentox.2012.01.007.

88. Rager JE, Auerbach SS, Chappell GA, Martin E, Thompson CM, Fry RC. 2017. Benchmark dose modeling estimates of the concentrations of inorganic arsenic that induce changes to the neonatal transcriptome, proteome, and epigenome in a pregnancy cohort. Chem Res Toxicol 30(10):1911–1920, PMID: 28927277, https://doi.org/10.1021/acs.chemrestox.7b00221.

89. Xi Y, Zhang Y, Zhu S, Luo Y, Xu P, Huang Z. 2020. PPAR-mediated toxicology and applied pharmacology. Cells 9(2):352, PMID: 32028670, https://doi.org/10.3390/cells9020352.

90. Cullingford TE, Bhakoo K, Peuchen S, Dolphin CT, Patel R, Clark JB. 1998. Distribution of mRNAs encoding the peroxisome proliferator-activated receptor α, β, and γ and the retinoid X receptor α, β, and γ in rat central nervous system. J Neurochem 70(4):1366–1375, PMID: 9523552, https://doi.org/10.1046/j.1471-4159.1998.70041366.x.

91. Hsieh YC, Chiang MC, Huang YC, Yeh TH, Shih HY, Liu HF, et al. 2018. Pparα deficiency inhibits the proliferation of neuronal and glial precursors in the zebrafish central nervous system. Dev Dyn 247(12):1264–1275, PMID: 30358936, https://doi.org/10.1002/dvdy.24683.

92. Thisse B, Thisse C. 2008. Data from: expression from: unexpected novel relational links uncovered by extensive developmental profiling of nuclear receptor expression. *ZFIN Direct Data Submission*. http://zfin.org [accessed 26 June 2024].

93. Christou M, Fraser TWK, Berg V, Ropstad E, Kamstra JH. 2020. Calcium signaling as a possible mechanism behind increased locomotor response in zebrafish larvae exposed to a human relevant persistent organic pollutant mixture or PFOS. Environ Res 187:109702, PMID: 32474314, https://doi.org/10.1016/j.envres.2020.109702.

94. Heintz MM, Chappell GA, Thompson CM, Haws LC. 2022. Evaluation of transcriptomic responses in livers of mice exposed to the short-chain PFAS compound HFPO-DA. Front Toxicol 4:937168, PMID: 35832492, https://doi.org/10.3389/ftox.2022.937168.

95. Rosen MB, Das KP, Rooney J, Abbott B, Lau C, Corton JC. 2017. PPARα-independent transcriptional targets of perfluoroalkyl acids revealed by transcript profiling. Toxicology 387:95–107, PMID: 28558994, https://doi.org/10.1016/j.tox.2017.05.013.

96. Houck KA, Patlewicz G, Richard AM, Williams AJ, Shobair MA, Smeltz M, et al. 2021. Bioactivity profiling of per- and polyfluoroalkyl substances (PFAS) identifies potential toxicity pathways related to molecular structure. Toxicology 457:152789, PMID: 33887376, https://doi.org/10.1016/j.tox.2021.152789.

97. Costello E, Rock S, Stratakis N, Eckel SP, Walker DI, Valvi D, et al. 2022. Exposure to per- and polyfluoroalkyl substances and markers of liver injury: a systematic review and meta-analysis. Environ Health Perspect 130(4):046001, PMID: 35475652, https://doi.org/10.1289/EHP10092.

98. Ankley GT, Bennett RS, Erickson RJ, Hoff DJ, Hornung MW, Johnson RD, et al. 2010. Adverse outcome pathways: a conceptual framework to support ecotoxicology research and risk assessment. Environ Toxicol Chem 29(3):730–741, PMID: 20821501, https://doi.org/10.1002/etc.34.

99. Tollefsen KE, Scholz S, Cronin MT, Edwards SW, de Knecht J, Crofton K, et al. 2014. Applying Adverse Outcome Pathways (AOPs) to support Integrated Approaches to Testing and Assessment (IATA). Regul Toxicol Pharmacol 70(3):629–640, PMID: 25261300, https://doi.org/10.1016/j.yrtph.2014.09.009.

100. Bal-Price A, Crofton KM, Leist M, Allen S, Arand M, Buetler T, et al. 2015. International STakeholder NETwork (ISTNET): creating a developmental neurotoxicity (DNT) testing road map for regulatory purposes. Arch Toxicol 89(2):269–287, PMID: 25618548, https://doi.org/10.1007/s00204-015-1464-2.

101. Villeneuve DL, Mueller ND, Martinović D, Makynen EA, Kahl MD, Jensen KM, et al. 2009. Direct effects, compensation, and recovery in female fathead minnows exposed to a model aromatase inhibitor. Environ Health Perspect 117(4):624–631, PMID: 19440503, https://doi.org/10.1289/ehp.11891.

102. Heasman J. 2002. Morpholino oligos: making sense of antisense? Dev Biol 243(2):209–214, PMID: 11884031, https://doi.org/10.1006/dbio.2001.0565.

103. Smits AH, Ziebell F, Joberty G, Zinn N, Mueller WF, Clauder-Münster S, et al. 2019. Biological plasticity rescues target activity in CRISPR knock outs. Nat Methods 16(11):1087–1093, PMID: 31659326, https://doi.org/10.1038/s41592-019-0614-5.

104. Chiavacci E, Kirchgeorg L, Felker A, Burger A, Mosimann C. 2017. Early frameshift alleles of zebrafish *tbx5a* that fail to develop the heartstrings phenotype. bioRxiv. Preprint posted online 7 March 2017, https://doi.org/10.1101/103168v2.

105. Schuermann A, Helker CSM, Herzog W. 2015. Metallothionein 2 regulates endothelial cell migration through transcriptional regulation of *vegfc* expression.

Angiogenesis 18(4):463–475, PMID: 26198291, https://doi.org/10.1007/s10456-015-9473-6.

106. Girroir EE, Hollingshead HE, He P, Zhu B, Perdew GH, Peters JM. 2008. Quantitative expression patterns of peroxisome proliferator-activated receptor-β/δ (PPARβ/δ) protein in mice. Biochem Biophys Res Commun 371(3):456–461, PMID: 18442472, https://doi.org/10.1016/j.bbrc.2008.04.086.

107. Warden A, Truitt J, Merriman M, Ponomareva O, Jameson K, Ferguson LB, et al. 2016. Localization of PPAR isotypes in the adult mouse and human brain. Sci Rep 6:27618, PMID: 27283430, https://doi.org/10.1038/srep27618.

108. Dickey AS, Pineda VV, Tsunemi T, Liu PP, Miranda HC, Gilmore-Hall SK, et al. 2016. PPAR-δ is repressed in Huntington's disease, is required for normal neuronal function and can be targeted therapeutically. Nat Med 22(1):37–45, PMID: 26642438, https://doi.org/10.1038/nm.4003.

109. Den Broeder MJ, Kopylova VA, Kamminga LM, Legler J. 2015. Zebrafish as a model to study the role of peroxisome proliferating-activated receptors in adipogenesis and obesity. PPAR Res 2015:358029, PMID: 26697060, https://doi.org/10.1155/2015/358029.

110. OECD (Organisation for Economic Co-operation and Development). 2007. *Test No. 426: developmental Neurotoxicity Study, OECD Guidelines for the Testing of Chemicals, Section 4*. Paris, France: OECD Publishing. https://doi.org/10.1787/9789264067394-en.

111. US EPA. 1998. *Health Effects Test Guidelines: OPPTS 870.6300 Developmental Neurotoxicity Study*. EPA 712-C-98-239. Washington, DC: US EPA.

112. Fleischer M. 2007. Research paper: testing costs and testing capacity according to the REACH requirements—results of a survey of independent and corporate GLP laboratories in the EU and Switzerland. J Bus Chem 4(3):96–114.

113. Makris SL, Raffaele K, Allen S, Bowers WJ, Hass U, Alleva E, et al. 2009. A retrospective performance assessment of the developmental neurotoxicity study in support of OECD test guideline 426. Environ Health Perspect 117(1):17–25, PMID: 19165382, https://doi.org/10.1289/ehp.11447.

114. Paparella M, Bennekou SH, Bal-Price A. 2020. An analysis of the limitations and uncertainties of in vivo developmental neurotoxicity testing and assessment to identify the potential for alternative approaches. Reprod Toxicol 96:327–336, PMID: 32781019, https://doi.org/10.1016/j.reprotox.2020.08.002.

115. Wang Z, Walker GW, Muir DCG, Nagatani-Yoshida K. 2020. Toward a global understanding of chemical pollution: a first comprehensive analysis of national and regional chemical inventories. Environ Sci Technol 54(5):2575–2584, PMID: 31968937, https://doi.org/10.1021/acs.est.9b06379.

116. Masjosthusmann S, Blum J, Bartmann K, Dolde X, Holzer AK, Stürzl LC, et al. 2020. Establishment of an a priori protocol for the implementation and interpretation of an in-vitro testing battery for the assessment of developmental neurotoxicity. EFSA Support Publ 17(10):1938E, https://doi.org/10.2903/sp.efsa.2020.EN-1938.

117. Carstens KE, Carpenter AF, Martin MM, Harrill JA, Shafer TJ, Paul Friedman K. 2022. Integrating data from *in vitro* new approach methodologies for developmental neurotoxicity. Toxicol Sci 187(1):62–79, PMID: 35172012, https://doi.org/10.1093/toxsci/kfac018.

118. Brown JP, Hall D, Frank CL, Wallace K, Mundy WR, Shafer TJ. 2016. Editor's highlight: evaluation of a microelectrode array-based assay for neural network ontogeny using training set chemicals. Toxicol Sci 154(1):126–139, PMID: 27492221, https://doi.org/10.1093/toxsci/kfw147.

119. Shafer TJ, Brown JP, Lynch B, Davila-Montero S, Wallace K, Paul Friedman K. 2019. Evaluation of chemical effects on network formation in cortical neurons grown on microelectrode arrays. Toxicol Sci 169(2):436–455, PMID: 30816951, https://doi.org/10.1093/toxsci/kfz052.

120. Roberts AC, Bill BR, Glanzman DL. 2013. Learning and memory in zebrafish larvae. Front Neural Circuits 7:126, PMID: 23935566, https://doi.org/10.3389/fncir.2013.00126.

121. Teixidó E, Kießling TR, Krupp E, Quevedo C, Muriana A, Scholz S. 2019. Automated morphological feature assessment for zebrafish embryo developmental toxicity screens. Toxicol Sci 167(2):438–449, PMID: 30295906, https://doi.org/10.1093/toxsci/kfy250.